A Thesis on

STUDY OF MICROCHANNEL REACTOR USING CFD ANALYSIS

Submitted By

Stutee Bhoi

Roll No. 210CH1037

for the partial fulfillment of

Master of Technology

in

Chemical Engineering

Under the Supervision of

Prof. (Dr.)BasudebMunshi

Department of Chemical Engineering

National Institute of Technology

Rourkela

DEPARTMENT OF CHEMICAL ENGINEERING

NATIONAL INSTITUTE OF TECHNOLOGY, ROURKELA

ORISSA, INDIA - 769008

CERTIFICATE

This is to certify that the thesis titled "***Study of Microchannel Reactor using CFD Analysis***", submitted to the National Institute of Technology, Rourkela by **Stutee Bhoi**, Roll No. **210CH1037** for the award of the degree of **Master of Technology** in Chemical Engineering, is a bona fide record of research work carried out by her under my supervision and guidance. The candidate has fulfilled all the prescribed requirements. The thesis, which is based on candidate's own work, has not been submitted elsewhere for a degree/diploma.

Date: 26/05/12

Prof.(Dr.) Basudeb Munshi

Associate Professor
Department of Chemical Engineering
National Institute of Technology, Rourkela

ACKNOWLEDGEMENT

I take this opportunity to express my sense of gratitude and indebtedness to **Prof. Basudeb Munshi** for helping me a lot to complete the project, without whose sincere and kind effort, this project would not have been success.

I am also thankful to all the staff and faculty members of Chemical Engineering Department, National Institute of Technology, Rourkela for their consistent encouragement.

Date: 26/05/12

Stutee Bhoi
Roll. No.: 210CH1037
4th Semester, M. Tech
Chemical Engineering Dept

INDEX

ABSTRACT

Microchannel reactors involve reaction chamber whose dimensions are typically in the range of micrometers (µm) with volumetric capacity in the range of micro liters (µL). The high surface to volume ratio, efficient heat and mass transfer characteristics and vastly improved fluid mixing allow precision control of reaction with improved conversions, selectivities and yields of desired products. Reverse-flow action is used to utilize the thermal energy inside a reactor. Energy from the reaction and exit gasses are captured and utilized within the reactor by the reversing flow action. The captured thermal energy can be used to preheat the feed or can be extracted from the reactor. The present work is aimed to study the behavior of combustion reaction of methane and propane inside a microchannel reactor. The advantages of reverse flow reactor have been found out by studying the phenomenon inside a reverse flow reactor. Both steady state and transient simulations has been carried out. Steady state solution was used as the basis for transient solution. The transient solution shows the presence of cyclic steady state temperature profile inside the reactor. The result reveals that the temperature of the gas increases with axial length, reaches maximum and then decreases. With increase in inlet temperature, maximum temperature of the fluid increases. Besides, the temperature peak decreases with increase in mass diffusivity of the mixture and wall heat transfer coefficient. It is also observed that the reaction starts near the wall and then proceed towards the center.

Keywords: CFD, Reverse flow reactor, Microchannel reactor

LIST OF FIGURES

LIST OF TABLES

Page no.

NOMENCLATURE

ρ	density of fluid
p	static pressure
∇	Gradient
E	activation energy
μ	viscosity
v	velocity
t	time
g	acceleration due to gravity
Y_i	mass fraction
D	diffusion coefficient
Sc	Schmidt number
M	molecular weight
ν	stochiometric coefficient
C	concentration
η	rate exponent
T	temperature
α	volume fraction
R	rate of the reaction
k	rate constant
Subscripts	
j	species
t	turbulent
r	reaction
p,q	phase

CHAPTER 1

INTRODUCTION

Chapter 1

INTRODUCTION

Microchannel reactor involves reaction chamber whose dimensions are typically in the range of micrometers (μm) with volumetric capacity in the range of micro liters (μL). It is usually a continuous flow reactor. Microreactors can be used to synthesize material more effectively than current batch techniques due to efficient heat and mass transfer characteristics, vastly improved fluid mixing, high surface area to volume ratio environment as well as engineering advantages in handling unstable intermediates. It can involve liquid-liquid systems but also involve solid-liquid systems, for example the channel walls coated with a heterogeneous catalyst. These reactors offer many advantages over conventional scale reactors such as vast improvements in reaction speed, energy efficiency and yield, reliability, safety, scalability and a much finer degree of process control. Microchannel reactors can remove heat much more efficiently than vessels. Hot spot temperatures as well as the duration of high temperature exposition due to exothermicity decreases remarkably. Thus, microreactors allow better kinetic investigations, because the local temperature gradients affecting reaction rates are much smaller compared to any batch vessel. Besides, heating and cooling a microreactor is also much quicker and operating temperatures can be as low as −100 °C. As a result of the efficient heat transfer, reaction temperatures may be much higher compared to conventional batch-reactors. Many low temperature reactions can be performed in microreactors at temperatures of −10 °C rather than −50 °C to −78 °C as in laboratory glassware equipment. Microreactors are generally operated continuously. This allows the subsequent processing of unstable intermediates and avoids typical batch workup delays. The rapid work up avoids decay of precious intermediates and often allows better selectivity. But microreactors generally do not tolerate particulates well and often clogging occurs. These are well suitable for fast and exothermic reactions but cause trouble as soon as particles are involved (Gokhale et al, 2005).

1.1 ADVANTAGES OF MICROCHANNEL REACTOR

Some of the advantages of microchannel reactors are listed below (Gokhale et al, 2005):

Improved surface-area-to-volume ratio: The ratio in case of a typical microreactor surface is about 200 cm^2 cm^{-3}, compared with 1 cm^2 cm^{-3} for a 100 mL glass flask and 0.06 cm^2 cm^{-3} for a 1 m^3 batch reactor.

Efficient mixing: Heat transfer and mass transport is improved considerably in microreactors. In microreactors mixing occurs through diffusion between laminar flow layers. Highly exothermic reactions can be performed under isothermal conditions due to the high heat exchanging efficiency. The accumulation of reaction heat and development of hot spots within the microreactor are suppressed so that fragmentation and undesirable side reactions are hindered.

Small reaction volumes: In case of reactions that take place in small volumes, process parameters such as temperature, pressure, residence time, and flow rate are more easily controlled. The hazardous effect of explosive reactions or strongly exothermic can also be drastically reduced. Higher safety can also be attained with toxic substances.

1.2 APPLICATION OF MICROCHANNEL REACTOR

Applications of microchannel reactors range from the production of commodity chemicals such as ethylene oxide, vinyl acetate, acrylonitrile and acrylic acid via selective partial oxidation reactions to steam methane reforming to produce hydrogen for use in fuel cells. Microrreactors are also used in biogas reforming processes for syngas production and in Fischer-Tropsch synthesis for biodiesel production. In addition it is also used for H_2O_2 production (Gokhale et al, 2005).

1.3 COMPUTATIONAL FLUID DYNAMICS

Fluid (gas and liquid) flows are governed by partial differential equations (PDE) which represent conservation laws for the mass, momentum and energy. Computational Fluid Dynamics (CFD) is

used to replace such PDE systems by a set of algebraic equations which can be solved using digital computers. The basic principle behind CFD modeling method is that the simulated flow region is divided into small cells. Differential equations of mass, momentum and energy balance are discretized and represented in terms of the variables at any predetermined position within the or at the center of cell. These equations are solved iteratively until the solution reaches the desired accuracy (ANSYS Fluent 12.0). CFD provides a qualitative prediction of fluid flows by means of

- mathematical modeling (partial differential equations)
- numerical methods (discretization and solution techniques)
- software tools (solvers, pre- and postprocessing utilities)

1.3.1 ANSYS FLUENT SOFTWARE

FLUENT is one of the widely used CFD software package. ANSYS FLUENT software contains the wide range of physical modeling capabilities which are needed to model flow, turbulence, reactions and heat transfer for industrial applications. Features of ANSYS FLUENT software:

- TURBULENCE: ANSYS FLUENT offers a number of turbulence models to study the effects of turbulence in a wide range of flow regimes.
- MULTIPHASE FLOW: It is possible to model different fluids in a single domain with FLUENT.
- ACOUSTICS: It allows users to perform sound calculations.
- REACTING FLOW: Modelling of surface chemistry, combustion as well as finite rate chemistry can be done in fluent.
- MESH FLEXIBILITY: ANSYS FLUENT software provides mesh flexibility. It has the ability to solve flow problems using unstructured meshes. Mesh types that are supported in FLUENT includes triangular, quadrilateral, tetrahedral, hexahedral, pyramid, prism (wedge) and polyhedral. The techniques which are used to create polyhedral meshes save time due to its automatic nature. A polyhedral mesh contains fewer cells than the corresponding tetrahedral mesh. Hence convergence is faster in case of polyhedral mesh.

- DYNAMIC AND MOVING MESH: The user sets up the initial mesh and instructs the motion, while FLUENT software automatically changes the mesh to follow the motion instructed.
- POST-PROCESSING AND DATA EXPORT: Users can post-process their data in FLUENT software, creating among other things contours, path lines, and vectors to display the data.

1.4 OBJECTIVES OF THE PRESENT STUDY

The objective of present work is to study the following aspects of

- Computational Fluid Dynamics modeling and simulation of combustion of propane inside a microburner.
- Computational Fluid Dynamics modeling and simulation of combustion of methane inside a reverse flow reactor.

1.5 PLAN OF THE THESIS

Chapter 1 represents the complete introduction of the present study including the definition of microchannel reactor, its advantages and application and role of computational fluid dynamics

Chapter 2 deals with the literature review of microchannel reactor. This chapter is divided into the sections namely, combustion, microchannel reactor, combustion in microchannel reactor and reverse flow reactor.

Chapter 3 comprises of modeling equation of single phase and multiple phase flow. The model equation includes the equation of continuity, momentum and energy.

Chapter 4 represents the study of microburner using CFD. Here combustion of propane is taken as the model reaction. A two-dimensional computational fluid dynamics model of a microburner is solved to study the effects of microburner wall conductivity on combustion characteristics.

Chapter 5 constitutes of the study of reverse flow reactor using CFD. Combustion of methane is considered as the model reaction. A packed bed model is considered.

Chapter 6 deals with the overall conclusion

CHAPTER 2

LITERATURE REVIEW

Chapter 2

LITERATURE REVIEW

A lot of research has been done on microchannel reactor, both experimentally and numerically. This chapter deals with the literature review of microchannel reactor and it is divided into four sections:

- Combustion
- Microchannel reactor
- Combustion in microchannel reactor
- Reverse flow reactor

2.1 COMBUSTION

Combustion is defined as the sequence of exothermic chemical reactions between a fuel and an oxidant which is accompanied by the production of heat and conversion of chemical species. Below is the review on combustion that has been completed.

Wierzchowski et al., (2002) studied the carbon monoxide oxidation and methane combustion on gallium (III) oxide (Ga_2O_3), tin (IV) oxide (SnO_2) or vanadium pentoxide (V_2O_5) supported on γ -Al_2O_3 catalysts under the stoichiometric conditions. They found that the catalytic activity depends on the pretreatment conditions of the catalyst.

Chan et al., (2005) developed a two-dimensional unsteady-state heterogeneous model to simulate an oxygen permeable membrane reactor for partial oxidation of methane with steam added. They found that better performance in terms of high methane (CH_4) conversion, low carbon monoxide (CO) concentration and high hydrogen (H_2) yield can be achieved when the reactor operates at inlet gas temperature from 900 K to 1000 K, water to fuel (W/F) ratio of round 2 and gas hour space velocity of about 20000/h.

Deshmukh and Vlachos (2007) proposed a reduced mechanism and a one-step rate expression for fuel-lean methane/air catalytic combustion on an Rh catalyst. These were developed from a detailed micro kinetic model using a computer-aided model reduction strategy that employs sensitivity analysis, partial equilibrium analysis, reaction path analysis and simple algebra to figure out the most abundant reaction intermediate and the rate-determining step.

Liu et al., (2009) studied the combustion of methane–air mixtures in a two-section porous burner. They developed a numerical model and used the FLUENT software to solve the two-dimensional transient mathematical model of the combustion. They found that the contours of velocity and temperature change considerably at the interface of the porous media and near the wall. Besides, the gas temperature at the low inlet velocity limit is more than that for the high velocity limit. It was also found that the thermal conductivity in the upstream section has higher influence on the temperature than that in the downstream section.

Bakry et al., (2010) experimented to study the characteristics of combustion using a pre-mixed methane–air mixture within a non-homogeneous porous inert medium (PIM) under high pressure and temperature. They developed a flame stabilization technique in porous inert media (PIM) combustion under high pressure and temperature in order to obtain a stable flame under these operating conditions within PIM. The experiments covered a broad spectrum of operating conditions ranging from a mixture inlet temperature of 20 °C and pressure ratio of 1 up to a temperature of 400 °C and a pressure ratio of 9.

Feng et al., (2010) studied numerically on CH_4 and air premixed combustion inside a small tube with a temperature gradient at the wall. They investigated on the effects of inlet velocity, combustor size and equivalence ratio on combustion characteristics and found that the inlet velocity has a significant influence on the reaction zone. Besides, the flame front shifts downstream as the inlet velocity increase. Besides, the inlet velocity has no obvious effects on the flame temperature and the combustor size strongly influences the combustion characteristics.

Abbasi et al., (2012) performed a kinetic study over thermally aged and steam-aged Pt and Pt–Pd catalysts to investigate the effect of temperature and methane and water concentrations on the performance of catalysts in the range of interest for environmental applications. They found that both catalysts permanently lose a large portion of their initial activity as result of exposure to

5 vol.% water in the reactor feed. Based on the observations they adopted an empirical rate equation for methane combustion over Pt and Pt-Pd catalysts.

In case of methane combustion over Pt catalyst, reaction rate expression is given by

$$-R_{CH_4} = kC_{CH_4} = A\exp\left(\frac{-E}{R_gT}\right)C_{CH_4} \quad (2.1)$$

In case of methane combustion over Pt-Pd catalyst, reaction rate expression is given by

$$-R_{CH_4} = \frac{kC_{CH_4}}{1+K_{H_2O}C_{H_2O}} = \frac{A\exp\left(\frac{-E}{R_gT}\right)C_{CH_4}}{1+A_w\exp\left(\frac{\Delta H_{ads}}{R_gT}\right)C_{H_2O}} \quad (2.2)$$

The values of kinetic parameters for fresh and steam-aged Pt catalyst are given in table below

Table 2.1: Kinetic parameters for fresh and steam-aged Pt catalyst (Abbasi et al., 2012)

	A (s−1)	E (kJ/mol)
Fresh Pt catalyst	1.79×10^6	81.0
Steam-aged Pt catalyst	1.14×10^6	82.9

The values of kinetic parameters for fresh and steam-aged Pt–Pd catalyst are given in table below

Table 2.2: Kinetic parameters for fresh and steam-aged Pt–Pd catalyst (Abbasi et al., 2012)

	Low temp. region (below 545 ˚C)		High temp. region (above 545 ˚C)		Adsorption constants	
	A (s−1)	E (kJ/mol)	A (s−1)	E (kJ/mol)	A_W (m^3/mol)	ΔH_{ads} (kJ/mol)
Fresh Pt-Pd catalyst	1.99×10^7	78.2	-	-	0.0527	24.1
Steam-aged Pt-Pd catalyst	1.81×10^6	72.6	8.01×10^3	35.7	0.0527	24.1

2.2 MICROCHANNEL REACTOR

Microchannel chemical processing technology is an emerging field with applications in most industrial processes due to controlled reaction environment, energy efficiency and excellent mixing. This technology offers improvements in existing processes and enables new processes to become cost effective.

Triplett et al., (1999) experimented on the two phase flow pattern in microchannels. They conducted experiments using air and water in circular microchannels having 1.1 and 1.45 mm inner diameters, and in microchannels with semi-triangular (triangular with one corner smoothed) cross-sections having hydraulic diameters 1.09 and 1.49 mm.

Rouge et al., (2001) described the dehydration of iso-propanol to propane as a model reaction to study a microchannel reactor specially designed to operate in a periodic fashion and deposited with γ alumina as catalyst. They found that the catalyst coating does not change the

hydrodynamics and reactor can be operated in a periodic manner with frequencies up to 1 hertz with improved performance.

Wan et al., (2003) simulated the epoxidation reaction of 1-pentene to 1,2-epoxypentane with hydrogen peroxide in a titanium silicate-1 coated microchannel reactor. Reaction kinetics and the corresponding rate constant were calculated from the reaction data which was obtained from the batch reactor experiment using TS-1 zeolite grown on silicon wafer as catalyst. From the model and experimental results they found that a channel coated with a layer of TS-1 catalyst possessing high titanium content and small crystal size results in higher product yields.

Chen et al., (2004) developed a microchannel reactor coated with catalyst having high selectivity and activity. They found that potassium on supported Rh metal catalysts had a promoting effect in the CO selective catalytic oxidation under H_2 rich stream.

Liauw et al., (2005) compared the microchannels with fixed bed reactors. The selective oxidation of isoprene to citraconic anhydride over vanadia-supported catalysts was used as a test reaction for the comparison. They found that the success of micro channel reactors depends on the right choice of reactions and conditions and benefits from their outstanding characteristics such as extraordinary heat transfer rates, inherent safety to handle explosive mixtures and the possibility of integrating sensors or other processing steps such as mixing.

Zhang et al., (2006) studied the application of a stainless steel microchannel reactor for the continuous synthesis of zeolite NaA. They also studied the influence of some parameters like the residence time, the aging time of the synthesis solution and the crystallization temperature. They found that long aging time of the synthesis solution led to narrow particle size distribution and small mean particle size of the products in the microchannel reactor.

Adeosun et al., (2009) investigated the mixing behavior in laminar flow in microchannels using experimental and numerical approaches. The concept of residence-time distribution (RTD) was applied to indirectly characterize flow and mixing in a T-junction microchannel which was chosen as the model microchannel mixer/reactor. The study was done by performing computational fluid dynamics (CFD) simulations of pulse tracer experiments. They found that the CFD code in conjunction with the RTD measure can then be used as a predictive tool in the design, evaluation and optimization of microscale flow systems.

Aubin et al., (2009) investigated on the effect of microchannel aspect ratio (channel depth/channel width) on the axial dispersion coefficient and residence time distributions for Newtonian and shear-thinning non-Newtonian flow using computational fluid dynamics. The results showed that for a fixed cross-sectional area and throughput, narrowing of the residence time distribution occurs as the aspect ratio decreases.

Arzamendi et al., (2010) presented a three dimensional computational fluid dynamics of heat transfer in a microchannel reactor for the low temperature Fischer–Tropsch synthesis. The microreactor studied was a steel block with 80 square microchannels of 1 mm of side arranged in cross-flow configuration for the transport of syngas and cooling water. They found a significant effect of the buoyancy forces on the thermal performance of the microreactor.

Chu et al., (2010) investigated the flow characteristics in curved rectangular microchannels with different aspect ratios and curvature ratios for Re numbers ranging from 80 to 876. They found that the geometrical channel aspect ratio has a significant influence on the pressure drop and decreased value of channel curvature ratio results in higher pressure loss.

Bhangale et al., (2011) used microreactors to study enzyme-catalyzed ring-opening polymerization of Ɛ-caprolactone to polycaprolactone. They observed that faster polymerization was achieved in microreactors compared to batch reactors.

Choi et al., (2011) conducted experiments of water flow boiling in hydrophilic and hydrophobic rectangular microchannels to investigate the wettability effect on flow boiling in rectangular microchannels. Photosensitive glass was used to fabricate the rectangular microchannels to visualize flow pattern. The hydrophilic bare photosensitive glass microchannel was chemically treated to get a hydrophobic microchannel. They found that the boiling heat transfer coefficient in the hydrophobic rectangular microchannel was higher than that in the hydrophilic rectangular microchannel. And also found that the pressure drop in the hydrophobic rectangular microchannel was higher than that in the hydrophilic rectangular microchannel.

Karakaya et al., (2011) investigated the effect of parametric variation of geometric and material properties on the coupling of exothermic and endothermic reactions in parallel microchannels. Heat required for the endothermic reforming of iso-octane to produce hydrogen was provided by the catalytic combustion of methane. They modeled the combination of steam reforming and

combustion for a microchannel reactor configuration in which reactions and heat transfer take place in parallel, micro-sized, square shaped flow paths with wall-coated catalysts. The geometric parameters considered were side-length of the microchannels, thickness of the wall between microchannels and channel texture (i.e. straight-through, micro-baffled).

Kobayashi et al. (2011) presented the computational fluid dynamics (CFD) simulation and analysis of the generation of soybean oil- in-water emulsion droplets via asymmetric straight flow through microchannels. CFD was used to investigate the effects of the channel size on emulsification. It was found that the maximum droplet generation rate per channel was inversely proportional to the channel size, excepting that the buoyancy force did not promote droplet detachment.

Liu et al., (2011) studied forced convection heat transfer occurring in microchannel. The influence of microchannel geometric shape on heat transfer performance was investigated by evaluating fluid thermo physical parameter and Nusselt number of the high-temperature surface. The heat exchange efficiency increases with inlet Reynolds number. The results also indicate that the shield-shaped groove microchannel possesses the highest heat exchange performance and compared with the lowest heat transfer efficiency of the surface having plain structure, the averaged Nusselt number can be increased by 1.3 times.

Sotowa et al. (2011) studied the effect of indentations and baffles formed in a deep microchannel on the mixing performance. The study showed that the formation of indentations and baffles enhances the mixing rate in deep microchannel reactors.

2.3 COMBUSTION IN MICROCHANNEL REACTOR

Guan et al., (2008) investigated on the catalytic combustion of high concentrations of methane over Pd-loaded γ-Al_2O_3 catalysts coated in microchannels. Three types of γ-Al_2O_3 coating structures were prepared in microchannels: a well-defined ordered macroporous structure, a random macroporous structure and a structure without macropores (dense structure). The incipient wetness impregnation method was used to load Pd-based catalysts on the coatings prepared. The results for the catalytic combustion of methane indicated that the catalysts

supported on coatings with a random or ordered macroporous structure showed better reactive activity than those on coatings with a dense structure.

Gandia et al., (2009) presented the thermal integration of the steam reforming of methanol (SRM) and the combustion of methanol in a catalytic microchannel reactor. They carried out a three dimensional simulation under relevant conditions.

Men et al., (2009) studied the combustion of propane on wash-coated noble metal supported catalysts in a catalytic microchannel combustor under different reaction conditions in the temperature range of 250–750 °C. It was found that at 325 °C reaction temperature and at a space velocity of 300 NL/(h gcat) full propane conversion could be achieved over Pt/MoO_x /Al_2O_3 catalyst in the slight excess of oxygen.

Chao et al., (2010) proposed a novel design concept for the enhancement of methane combustion inside a microchannel that uses the combined effects of catalyst segmentation and cavities. Their objective of using catalyst segmentation and cavities in a micro-reactor was to integrate the advantages of the heterogeneous and homogeneous reactions to enhance fuel conversion and to promote complete combustion in a confined distance. It was found that cavities can appreciably extend the stable operational range of the microreactor for a wide range of inlet flow rates.

Zhang et al., (2011) used a quartz annular flow microreactor for the experimental investigation of the gas phase partial methane oxidation to formaldehyde under high temperature (1173–1273 K) and short residence time (20–60 ms). The microreactor having annular space 0.5 mm wide was used vertically. The microreactor was heated by three independent thermocoax resistance wires. Downstream the heating zone, the indirect quenching was performed by a heat exchanger located on the periphery of the external tube of the annular zone. Under this experimental condition, high formaldehyde selectivity (up to 80%) was achieved, but the yield remained low.

Irani et al., (2011) presented two approaches for reaction modeling in monolith reactors. In the first approach, the reactions were assumed to take place on the wall surfaces, while in the second approach penetration and reaction of chemical species inside a thin layer near the walls were of essential concern. Comparisons between modeling results and experimental data showed that the first approach (surface reactions) exhibits better results both in generality and accuracy.

2.4 REVERSE FLOW REACTOR

Reverse flow reactor is a reactor in which the flow direction is changed after every specified time. The reactor may be run as a traditional fixed-bed reactor. In the active part of the reactor a packed bed, monolith or other section may be used. There is also an inert section on either side of the catalyst section which is used to store thermal energy from the heat of reaction and that energy is used to preheat the inlet gas. The hot exit gas from the reactor heats up the exit inert layer, thereby storing thermal energy. Thus when the flow direction is reversed, the warm inert section now uses this stored thermal energy to preheat the feed. When the feed gas encounters the catalyst region, it has already warmed up from the inlet temperature. The gas now reacts at a slightly higher temperature, and with a slightly higher conversion, than if there was no preheat. The exit inert section on the other side now acquires the stored thermal energy during this phase of the cycle. After a specified time period, the flow direction is again reversed. As this cycle continues, the total amount of thermal energy stored in the reactor slowly increases until a pseudo-steady state regime is attained. Periodic flow reversal can be used to accumulate heat within the reactor, allowing the reactions to take place at a higher temperature. As the outer sections present in the either sides of the catalyst section tend to be cooler and have a less significant contribution to the reaction kinetics, these outer sections may be replaced with inert material. Inert material may have similar heat transfer properties as the catalyst, but may be many times cheaper to manufacture. The inert sections allow a reactor to be designed using less catalyst, lowering the overall capital investment in such a reactor (Salomons et al, 2004).

Gosiewski et al., (1999) presented a mathematical model of the reverse-flow reactor for the catalytic conversion of methane to synthesis gas. They developed a simple approximate procedure for the estimation of the effectiveness factor of the reactions, which enables the resistance due to internal diffusion to be taken into account at any point of the reactor without resorting to numerical integration of the diffusion equations in the pellet. A comparison was presented between the effectiveness factor obtained via the integration of the diffusion equations and that calculated using the linearized reaction rate equations.

Cittadini et al., (2001) investigated on the behavior of a reverse-flow combustor for the treatment of low-VOC (volatile organic compound) concentration waste gases, in the presence of periodical variations in the feed characteristics. Two kinds of variations were considered: in the

flow rate and in the inlet concentration. In both the cases, the variations cause consistent fluctuations in conversion and in the maximum temperature of the bed. These fluctuations, especially for long feeding cycle periods, can threaten the correct operation of the reactor. In addition to this, for particular ratios between the feeding cycle period and the flow-reversal cycle period, the interaction between this two cycles may cause serious problems of instability, represented by a dangerous flow asymmetry in the case of variations in the flow rate and by large low-frequency fluctuations of the maximum temperature in the case of variations in the inlet concentration.

Ramdani et al., (2001) studied the VOC combustion inside a medium-scale reverse flow reactor. The extinction limit was studied. Heat loss and dilution were found to be a crucial phenomenon.

Annaland et al., (2002) studied a new reactor concept for highly endothermic heterogeneously catalysed gas phase reactions at high temperatures having rapid but reversible catalyst deactivation. The aim of this reactor concept is to achieve an indirect coupling of energy required for endothermic reactions and energy released by exothermic reactions, without mixing the endothermic and exothermic reactants, in closed-loop reverse flow operation. This can be done by the incorporation of regenerative heat exchange inside the reactor via periodic gas flow reversals.

Glockler et al., (2003) studied the shortcomings of existing multifunctional reactor concepts for the autothermal coupling of endothermic and exothermic reactions. It was found that inefficient heat integration is the main reason which leads to excessive maximum temperatures or poor reactor performance.

Tullilah et al., (2003) compared experimental observations of flow-rate effects during ethylene oxidation on Pt or Al_2O_3, with simulations of this reactor using a kinetic rate expression. Adequate agreement was established between the experimental results and simulationed results, using homogeneous or heterogeneous reactor model with no adjustable parameters. The difference between the homogeneous and heterogeneous model predictions was usually small. The approximation shows that the most important parameters for predicting the highest temperature were the inert zone properties (conductivity and length).

Marin et al., (2004) compared systematically the performance of particle beds and monolithic beds in catalytic reverse flow reactors used for combustion of lean methane-air mixtures, using alumina-supported palladium as catalyst. Different values of particle diameter (3–6 mm, for particle bed), gas surface velocity (0.1–0.3 m/s), catalyst/inert ratio (0.4–1) and cell density (200–400 cpsi, for structured bed) were used for the simulation of the combustion of 3500 ppm methane in both kinds of reverse flow reactor. The results obtained indicate that the reverse flow reactor is more stable when the catalyst particle beds are used.

Salomons et al., (2004) described the development and validation of a computer simulator for the modeling of a reverse flow catalytic reactor for the combustion of lean mixtures of methane in air. A two dimensional heterogeneous model was used for the reactor. For catalytic sections packed bed and for inert sections ceramic monoliths were used. The transfer of energy was observed to be a significant factor in the reactor operation.

Chan et al., (2006) designed reverse-flow packed bed reactors to treat gaseous pollutants from chemical plants. The modified reverse-flow reactor (MRFR) was having a recuperator on each end of the reactor and a reaction zone in the middle.

Gosiewski et al., (2007) presented simulation results of a reverse-flow reactor for the catalytic combustion of methane that occurs in coal-mine ventilation air. Two methods for heat withdrawal were analyzed. The simulations indicate that a relation exists between the method for heat withdrawal and the asymmetry in the profiles of the catalyst temperature over half-cycles of flow reversal.

Liu et al., (2007) modeled a reverse flow catalytic converter used for a lean burn natural gas engine using FLUENT. A three dimensional model was used to study methane ignition. The complete methodology for the construction of pseudo-homogeneous and heterogeneous continuum models in the context of FLUENT was described. For the heterogeneous model, a dual zone approach was used, where double cells or nodes were used to distinguish between fluid and solid temperatures. The heterogeneous model requires more computational time than the pseudo-homogeneous model under unidirectional flow condition, and slightly more under reverse flow condition. It was found that for large changes in the inlet conditions, the use of a heterogeneous model is justified.

Marin et al., (2008) studied the application of reverse flow reactors for the combustion of lean mixtures of aliphatic and aromatic hydrocarbons in air. Hexane and toluene were chosen as model compounds. The combustion of binary mixtures of these compounds over a commercial Pt/Al_2O_3 catalyst in reverse flow reactors was studied both experimentally, in a bench scale unit, and by simulations.

Marin et al., (2009) worked on the application of monolithic catalysts and reverse flow reactor (RFR) technology for carrying out the water–gas shift reaction (WGS). The performance of both adiabatic fixed-bed reactors (FBR) and RFR operating with particulate or monolith catalysts has been simulated using a heterogeneous one- dimensional model. Comparisons were made at the same space velocities.

Zhenqiang et al., (2009) studied thermal oxidation of lean methane mixture inside a reverse flow reactor. Temperature field of flow fluid was coupled with temperature field of ceramic honeycomb. Influence of wall thickness and inlet velocity was determined numerically. It was found that thick wall leads to low temperature and low pressure loss and high inlet velocity leads to high temperature and high pressure loss.

CHAPTER 3

COMUTATIONAL FLUID DYNAMICS MODEL EQUATIONS

Chapter 3

COMPUTATIONAL FLUID DYNAMICS MODEL EQUATIONS

In this chapter the computational fluid dynamics modeling equations are described for single and multiphase system. Besides, reaction modeling equations are also mentioned. The theory for the system is taken from the ANSYS Fluent 12.0.

3.1 FLOW MODELLING

THE MASS CONSERVATION EQUATION

The equation for conservation of mass or continuity equation can be written as follows:

$$\frac{\partial \rho}{\partial t} + \nabla . (\rho \vec{v}) = 0 \tag{3.1}$$

Above equation is the general form of the mass conservation equation and is valid for incompressible as well as compressible flows.

MOMENTUM CONSERVATION EQUATIONS

The conservation of momentum equation is given by

$$\frac{\partial}{\partial t}(\rho \vec{v}) + \nabla . (\rho \vec{v} \vec{v}) = -\nabla p + \nabla . \left(\bar{\bar{\tau}}\right) + \rho \vec{g} + \vec{F} \tag{3.2}$$

where, p is the static pressure, $\bar{\bar{\tau}}$ is the stress tensor, and $\vec{g}$ and $\vec{F}$ are the gravitational body force and external body forces (e.g., that arise from interaction with the dispersed phase), respectively. $\vec{F}$ also contains other model-dependent source terms such as porous-media and user-defined sources.

The stress tensor $\bar{\bar{\tau}}$ is given by

$$\bar{\bar{\tau}} = \mu \left[(\nabla \vec{v} + \nabla \vec{v}^{T}) - \frac{2}{3} \nabla . \vec{v} I \right] \tag{3.3}$$

where μ is the molecular viscosity, I is the unit tensor, and the second term on the right hand side is the effect of volume dilation.

SPECIES TRANSPORT EQUATIONS

$$\frac{\partial}{\partial t}(\rho Y_i) + \nabla.(\rho \vec{v} Y_i) = -\nabla.\vec{J}_i + R_i + S_i \quad (3.4)$$

R_i is the net rate of production of species i by chemical reaction and S_i is the rate of creation by addition from the dispersed phase plus any user-defined sources. An equation of this form will be solved for N-1 species where N is the total number of fluid phase chemical species present in the system. Since the mass fraction of the species must sum to unity, the Nth mass fraction is determined as one minus the sum of the N-1 solved mass fractions.

Mass Diffusion in Laminar Flows

Ji is the diffusion flux of species i, which arises due to concentration gradients.

$$\vec{J}_i = -\rho D_{i,m} \nabla Y_i \quad (3.5)$$

Mass Diffusion in Turbulent Flows

$$\vec{J}_i = -\left(\rho D_{i,m} + \frac{\mu_t}{Sc_t}\right) \nabla Y_i \quad (3.6)$$

3.2 REACTION MODELLING

3.2.1 LAMINAR FINITE-RATE MODEL

The laminar finite-rate model computes the chemical source terms using Arrhenius expressions, and ignores the effects of turbulent fluctuations. The net source of chemical species i due to reaction is computed as the sum of the Arrhenius reaction sources over the N_R reactions that the species participate in:

$$R_i = M_{w,i} \sum_{r=1}^{N_R} \hat{R}_{i,r} \quad (3.7)$$

where $M_{w,i}$ is the molecular weight of species i and $\hat{R}_{i,r}$ is the Arrhenius molar rate of creation/destruction of species i in reaction r.

General form of rth reaction:

$$\sum_{i=1}^{N} v'_{i,r} M_i \Leftrightarrow \sum_{i=1}^{N} v''_{i,r} M_i \tag{3.8}$$

For a non-reversible reaction, the molar rate of creation/destruction of species i in r^{th} reaction is given by

$$\hat{R}_{i,r} = \Gamma\left(v''_{i,r} - v'_{i,r}\right)\left(k_{f,r} \prod_{j=1}^{N} \left[C_{j,r}\right]^{\left(\eta'_{j,r} + \eta''_{j,r}\right)}\right) \tag{3.9}$$

For a reversible reaction, the molar rate of creation/destruction of species i in reaction r is given by

$$\hat{R}_{i,r} = \Gamma\left(v''_{i,r} - v'_{i,r}\right)\left(k_{f,r} \prod_{j=1}^{N} \left[C_{j,r}\right]^{\eta'_{j,r}} - k_{b,r} \prod_{j=1}^{N} \left[C_{j,r}\right]^{\eta''_{j,r}}\right) \tag{3.10}$$

Γ represents the net effect of third bodies on the reaction rate. This term is given by

$$\Gamma = \sum_{j}^{N} \gamma_{j,r} C_j \tag{3.11}$$

The forward rate constant for reaction r, $k_{f,r}$ is computed using the Arrhenius expression

$$k_{f,r} = A_r T^{\beta r} e^{-E_r/RT} \tag{3.12}$$

If the reaction is reversible, the backward rate constant for reaction r, $k_{b,r}$ is computed from the forward rate constant using the following relation:

$$k_{b,r} = \frac{k_{f,r}}{K_r} \tag{3.13}$$

where K_r is the equilibrium constant for the rth reaction.

3.2.2 EDDY DISSIPATION MODEL

Most fuels are fast burning, and the overall rate of reaction is controlled by turbulent mixing. In non-premixed flames, turbulence slowly mixes fuel and oxidizer into the reaction zones where they burn quickly. In premixed flames, the turbulence slowly mixes cold reactants and hot products into the reaction zones, where reaction occurs rapidly. In such cases, the combustion is said to be mixing-limited, and the complex and often unknown, chemical kinetic rates can be safely neglected.

The net rate of production of species i due to reaction r, $R_{i,r}$, is given by the smaller (i.e., limiting value) of the two expressions below:

$$R_{i,r} = \nu'_{i,r} M_{w,i} A \rho \frac{\epsilon}{k} \min_R \left(\frac{Y_R}{\nu'_{R,r} M_{w,R}} \right) \tag{3.14}$$

$$R_{i,r} = \nu'_{i,r} M_{w,i} AB \rho \frac{\epsilon}{k} \frac{\sum_P Y_P}{\sum_j^N \nu''_{j,r} M_{w,j}} \tag{3.15}$$

where, A and B are empirical constants having values equal to 4.0 and 0.5 respectively. Y_P refers to the mass fraction of product species and Y_R refers to the mass fraction of any particular reactant.

3.3 MODELLING MULTIPHASE FLOW

EULERIAN MODEL

The Eulerian multiphase model in FLUENT allows for the modeling of multiple separate, yet interacting phases. The phases can be liquids, gases, or solids in nearly any combination.

Conservation of Mass

The continuity equation for phase q is

$$\frac{\partial}{\partial t}(\alpha_q \rho_q) + \nabla.(\alpha_q \rho_q \vec{v}_q) = \sum_{p=1}^{n} (\dot{m}_{pq} - \dot{m}_{qp}) + S_q \tag{3.16}$$

where α_q is the volume fraction of q^{th} phase, $\vec{v}_q$ is the velocity of phase q and $\dot{m}_{pq}$characterizes the mass transfer from the p^{th} to q^{th} phase, and $\dot{m}_{qp}$characterizes the mass transfer from phase q to phase p. For the problem considered in chapter 5, mass transfer is not considered.

$$\dot{m}_{pq} = 0$$

$$\dot{m}_{qp} = 0$$

$$S_q = 0$$

Conservation of Momentum

The momentum balance for phase q is

$$\frac{\partial}{\partial t}(\alpha_q \rho_q \vec{v}_q) + \nabla.(\alpha_q \rho_q \vec{v}_q \vec{v}_q) = -\alpha_q \nabla p + \nabla.\bar{\bar{\tau}}_q + \alpha_q \rho_q \vec{g} + \sum_{p=1}^{n}(\vec{R}_{pq} + \dot{m}_{pq}\vec{v}_{pq} - \dot{m}_{qp}\vec{v}_{qp}) +$$

$$(\vec{F}_q + \vec{F}_{lift,q} + \vec{F}_{vm,q}) \quad (3.17)$$

where $\bar{\bar{\tau}}_q$ is the q^{th} phase stress-strain tensor, $\vec{F}_q$is an external body force,$\vec{F}_{lift,q}$is a lift force, $\vec{F}_{vm,q}$is a virtual mass force, $\vec{R}_{pq}$is an interaction force between phases, $\vec{v}_{pq}$is the interphase velocity,and p is the pressure shared by all phases.

$$\bar{\bar{\tau}}_q = \alpha_q \mu_q \left(\nabla \vec{v}_q + \nabla \vec{v}_q^{\,T}\right) + \alpha_q \left(\lambda_q - \frac{2}{3}\mu_q\right)\nabla.\vec{v}_q \quad (3.18)$$

where μ_q and λ_q are the shear and bulk viscosity of phase q.

Conservation of Energy

$$\frac{\partial}{\partial t}(\alpha_q \rho_q h_q) + \nabla.(\alpha_q \rho_q \vec{u}_q h_q) = -\alpha_q \frac{\partial p_q}{\partial t} + \bar{\bar{\tau}}_q : \nabla \vec{u}_q - \nabla.\vec{q}_q + S_q +$$

$$\sum_{p=1}^{n}(\vec{Q}_{pq} + \dot{m}_{pq}\vec{v}_{pq} - \dot{m}_{qp}\vec{v}_{qp}) \quad (3.19)$$

where h_q is the specific enthalpy of the q^{th} phase, $\vec{q}_q$is the heat flux, S_q is a source term that includes sources of enthalpy, Q_{pq} is the intensity of heat exchange between the p^{th} and q^{th} phases, and h_{pq} is the interphase enthalpy. In case of problem considered in chapter 5

$$\vec{q}_q = -\frac{k}{\rho C_P}\frac{\partial h}{\partial n} \quad (3.20)$$

n is the direction vector. For the problem considered, k =10 W/mK, ρ =580 kg/m^3, C_P = 850 J/kg-K

CHAPTER 4

COMBUSTION OF PROPANE INSIDE A MICROBURNER

Chapter 4

COMBUSTION OF PROPANE INSIDE A MICROBURNER

This chapter deals with the combustion of propane inside a microburner. The burner consists of two parallel plates that are infinitely wide. A two-dimensional computational fluid dynamics model of the microburner is considered.

4.1 PROBLEM STATEMENT

Combustion of propane inside a microburner is considered. Premixed, non-preheated propane/air mixtures are fed to the inlet of the microburner, and hot product gases exit the microburner. Reduced one-step propane combustion chemistry is used that assumes the irreversible combustion of propane (Vlachos et al., (2004):

$$C_3H_8 + 5O_2 \rightarrow 3CO_2 + 4H_2O$$

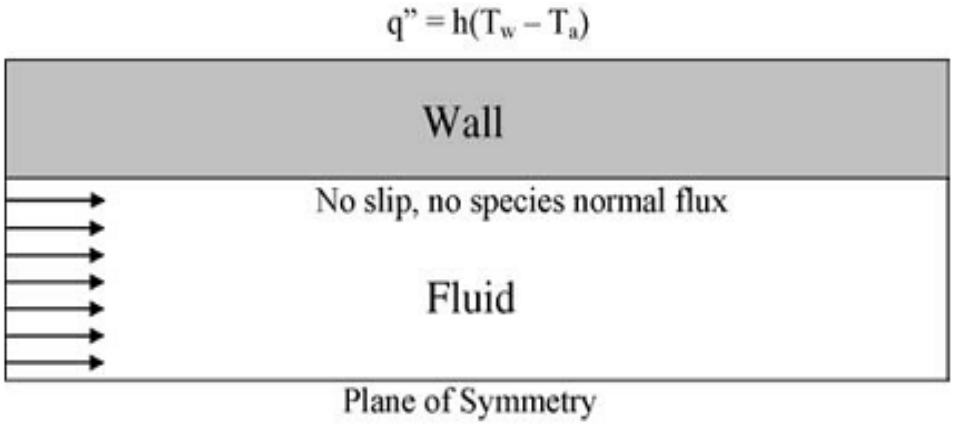

Figure 4.1: Computational domain (Vlachos et al., 2004)

Table 4.1: Operating conditions and model parameters used in simulation

Parameter	**Unit**	**Value**
Length	cm	1
Plate thickness	μm	200
Gap size	μm	600
Inlet temperature	K	300
Inlet velocity	m/s	0.5
Inlet mole fraction of propane		0.167

4.2 FLUENT SIMULATION

4.2.1 GEOMETRY AND MESH

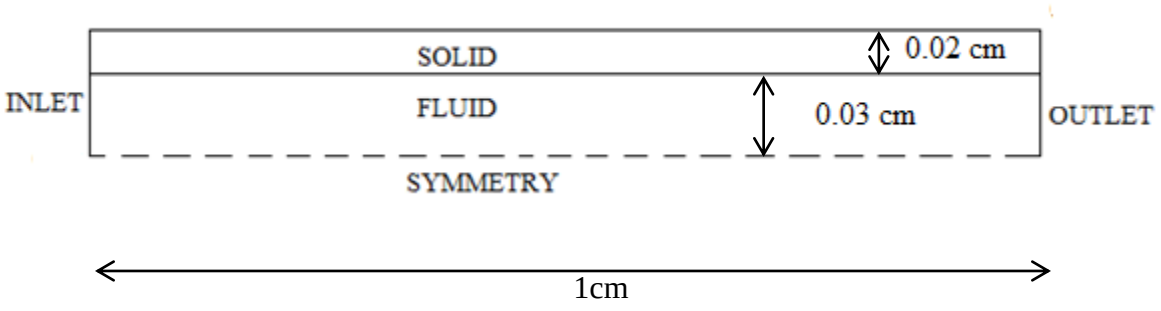

Figure 4.2: Schematic of computational domain

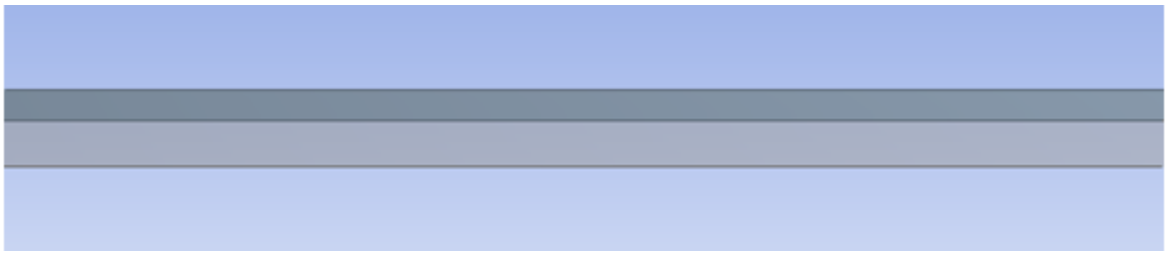

Figure 4.3: Geometry in ANSYS workbench

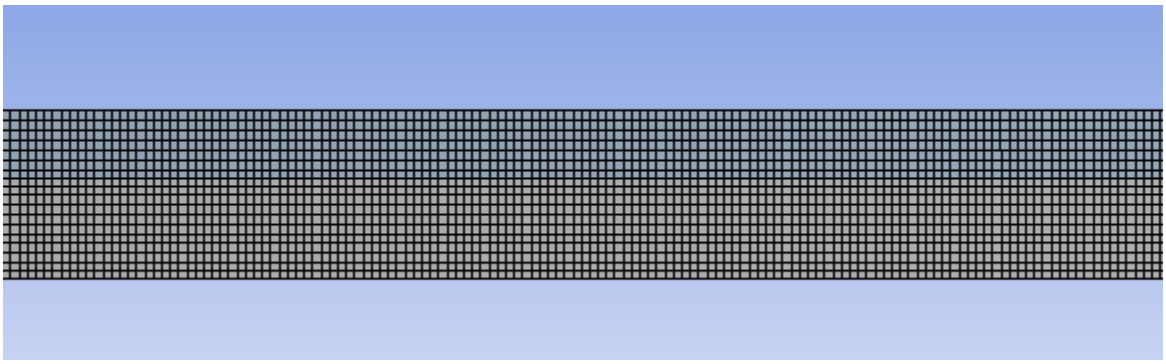

Figure 4.4: Meshing of geometry

A 2D geometry is created by using ANSYS 12 software. The geometry is created in ANSYS workbench. The geometry is meshed into smaller cells. Structured meshing method is used for meshing the geometry. It is meshed into 8020 nodes and 7200 elements.

4.2.2 BOUNDARY AND INITIAL CONDITIONS

In order to obtain a well-posed system of equation, reasonable boundary conditions for the computational domain have to be implemented. At inlet velocity of the mixture and mole fraction of the species are specified. At outlet pressure boundary condition is specified. Heat transfer coefficient is specified at the wall. No slip boundary condition is specified at the interface.

4.2.3 SOLUTION TECHNIQUES

In fluent, solver is set as segregated which solves the equation individually. Steady state simulation has been formulated. Here pressure based solver is used. The species transport model is considered. Eddy dissipation model is used to predict the reaction rate. The discretization scheme for momentum, turbulent dissipation rate, turbulent kinetic energy and all has been taken as first order upwind.

4.3 RESULTS AND DISCUSSION

In this section steady state simulation results are discussed. The temperature distributions of the gas inside the reactor along the axial as well as radial direction at specified positions are displayed. Besides, the concentration distribution of propane inside the reactor is also studied.

4.3.1 TEMPERATURE DISTRIBUTION

The contour plot of temperature has been shown below with the inlet velocity 0.5m/s, inlet temperature 300K, heat transfer coefficient 10 W/m^2K, wall thermal conductivity 0.5W/mK and stochiometric feed.

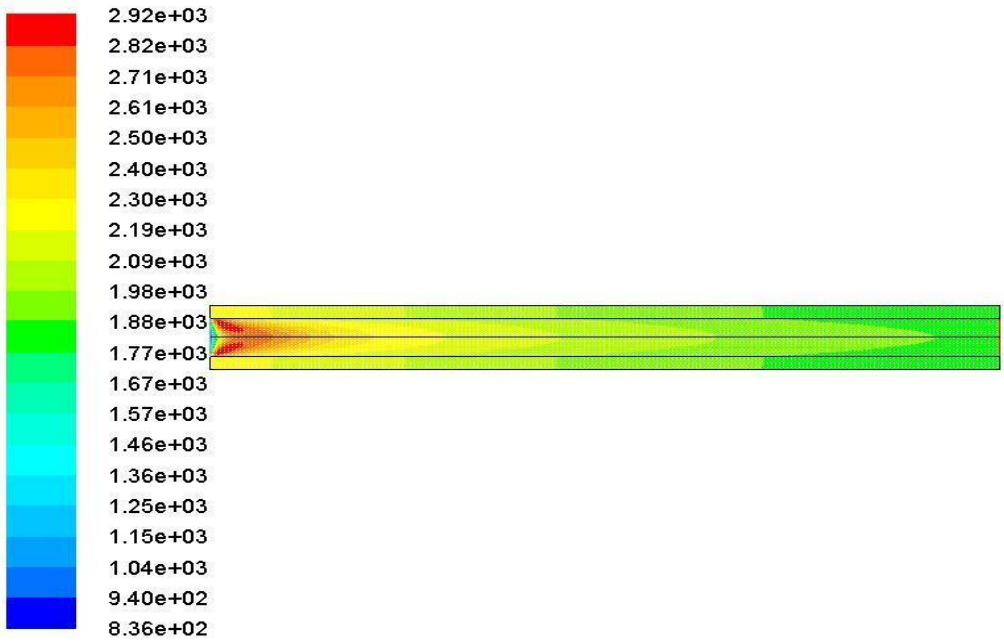

Figure 4.5: Contour plot of temperature (K), wall thermal conductivity = 0.5 W/mK

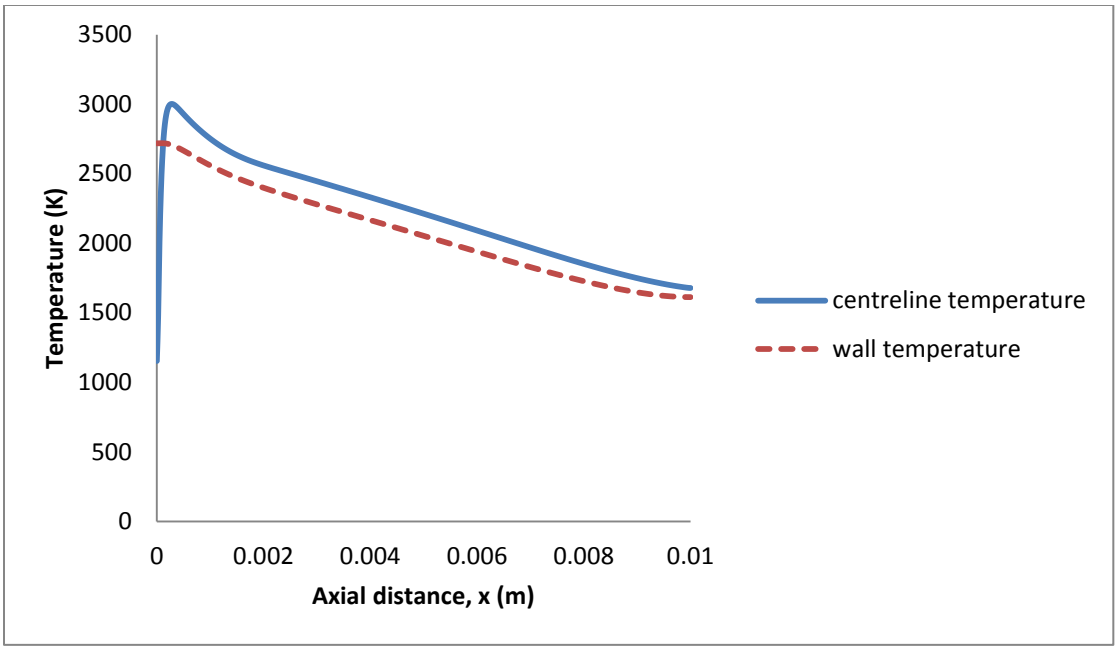

Figure 4.6: Temperature distribution along the axis for wall thermal conductivity = 0.5 W/mK

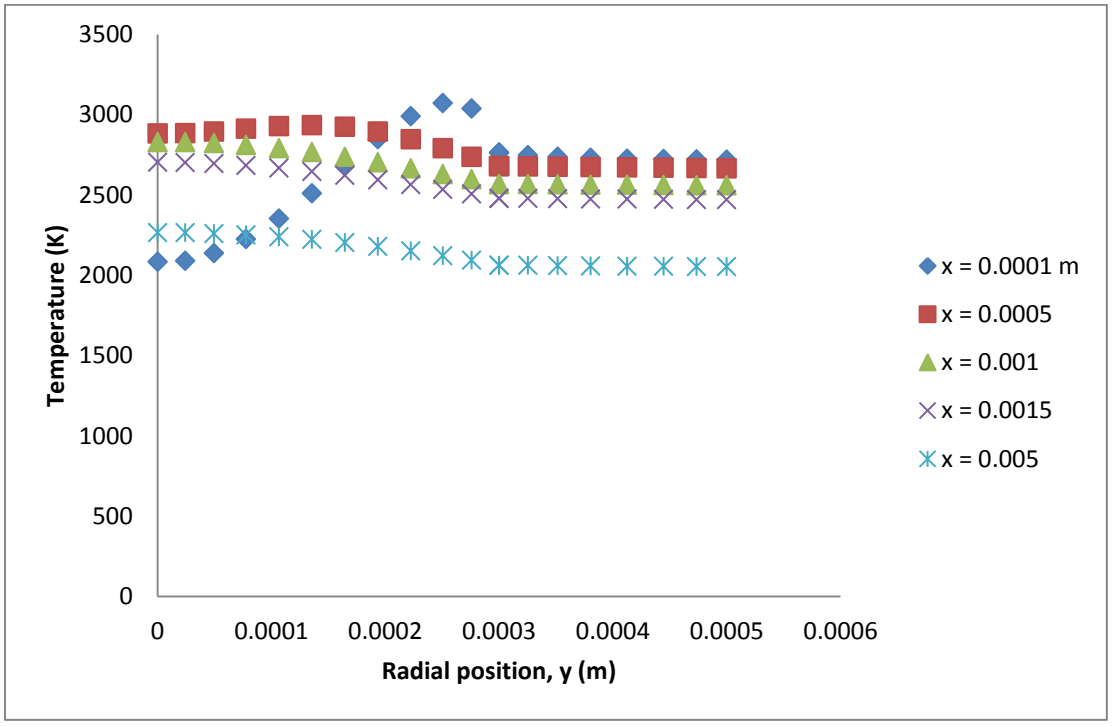

Figure 4.7: Steady state radial temperature distribution, wall thermal conductivity = 0.5 W/mK

Fig. 4.6 shows a comparison between axial distribution of centerline temperature and wall temperature. The centerline temperature varies with axial length. Near to the entry of the channel, temperature increases, reaches the maximum and then decreases. The temperature rise closer to the entry occurs due to the exothermicity of the reaction. The lower wall temperature as compared to the centerline temperature occurs due to more amount of combustion reaction around the center. The variation of temperature with radial position is depicted in Fig. 4.7. It is observed that the temperature of the gas near the center is the maximum except at radial distance 0.0001m. It is because the reaction first starts near the wall and then proceed towards the center. Due to the exothermicity of the reaction, the temperature is more near to the wall. It is observed that the temperature of the gas at the center is maximum in case of radial distance 0.0005 m.

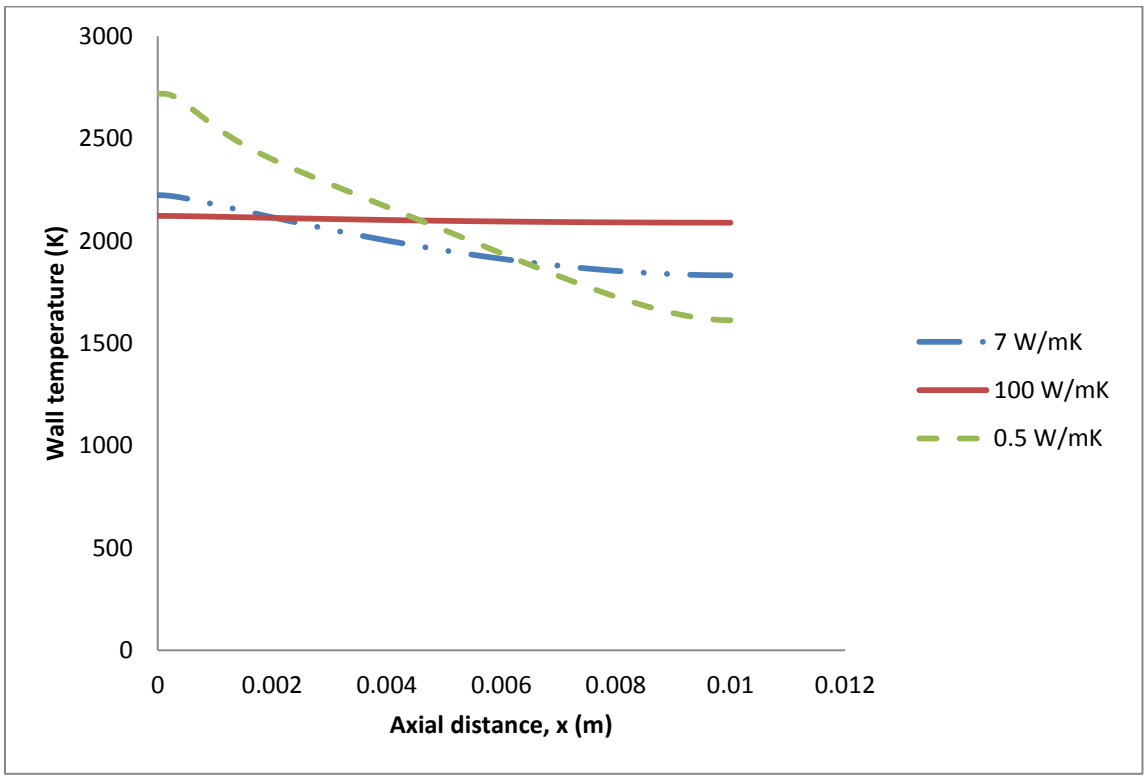

Figure 4.8: Wall outer edge temperature distribution

Fig. 4.8 shows the wall outer edge temperature distribution for different wall thermal conductivities. Low wall thermal conductivities result in large temperature gradient in axial direction and hence lager heat flux passes through the wall in the axial direction. This results in larger maximum temperature at lower thermal conductivity. The heat transfer resistance decreases with increase in thermal conductivity, and hence high wall thermal conductivity leads to uniform temperature profiles in axial direction without hotspots.

4.3.2 REACTION RATE DISTRIBUTION

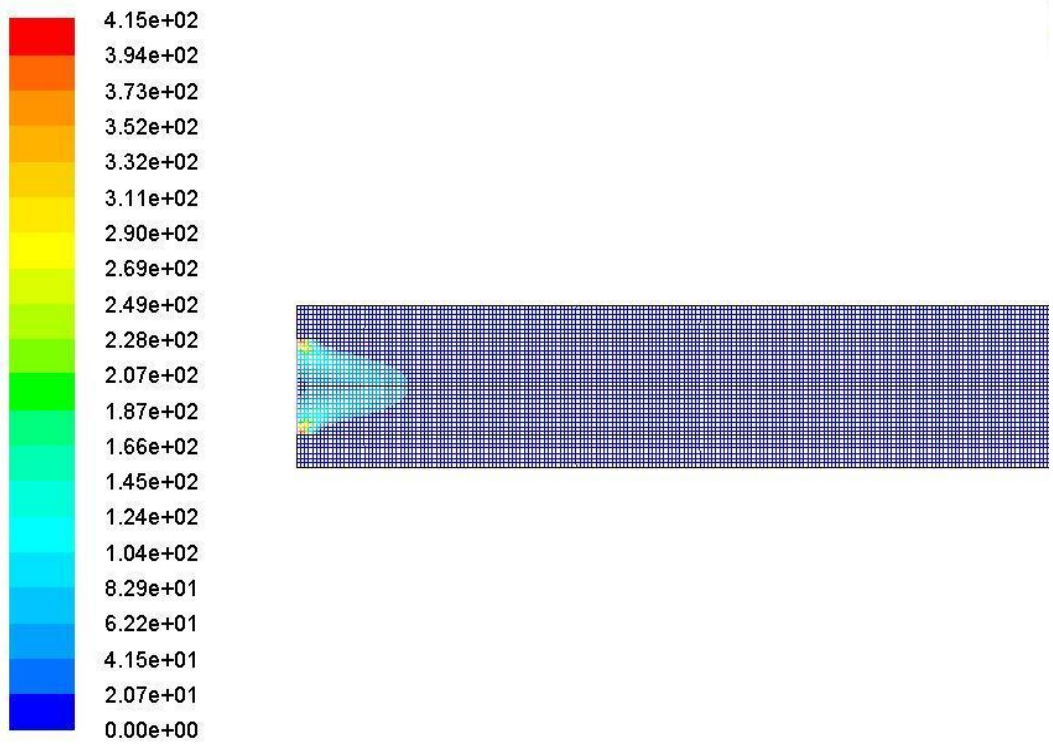

Figure 4.9: Contour plot of reaction rate (kmol/m^3-s)

The above figure shows the contour plot of reaction rate. Here for modeling reaction eddy dissipation model is considered. Near to the inlet the reaction rate is maximum.

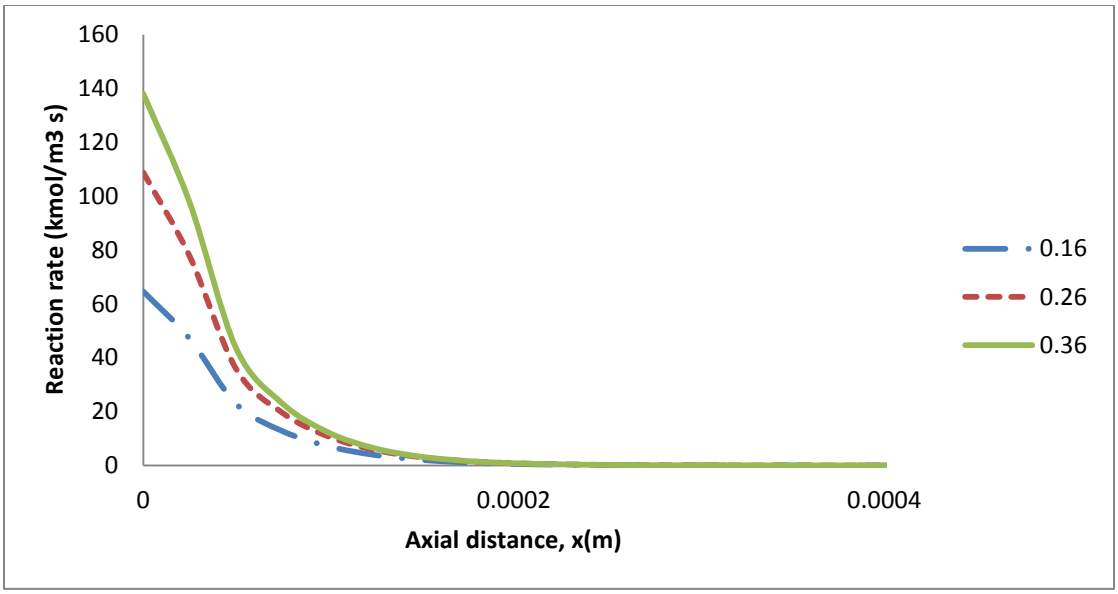

Figure 4.10: Reaction rate distribution for different mole fraction of propane

Fig. 4.10 shows the variation of the rate of reaction with axial distance for different inlet mole fraction of propane. The mixture is diluted with propane. It is observed that with increase in mole fraction of propane at the inlet the reaction rate also increases. The reaction rate expression in case of eddy dissipation model is mentioned in equation no. 3.14. According to the expression the reaction rate depends on the mass fraction of the reactant. From the figure it is observed that the reaction rate is maximum for inlet mole fraction of propane equal to 0.36

4.3.3 CONCENTRATION DISTRIBUTION

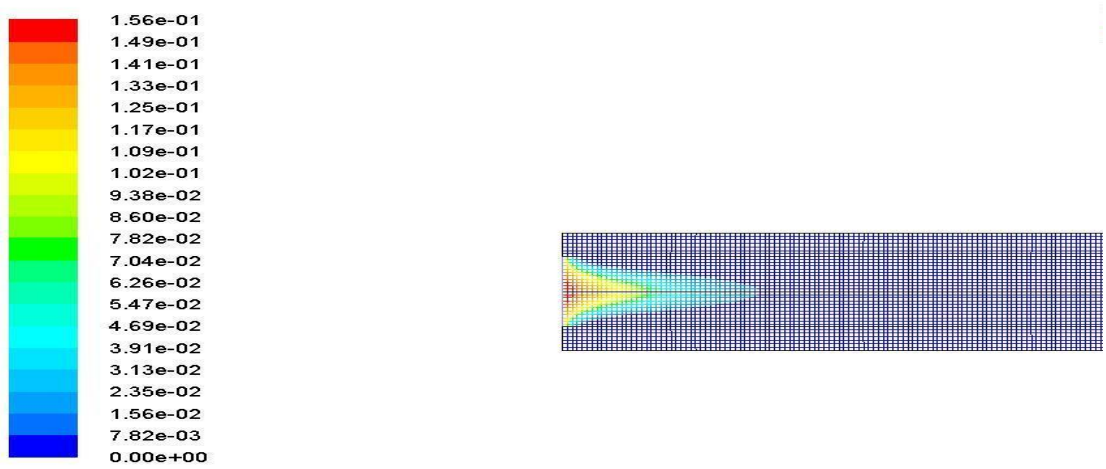

Figure 4.11: Contour plot of molar concentration of propane (kmol/m^3)

The contour plot of mole fraction of propane is shown in the Fig. 4.11. The mole fraction of propane decreases with axial length. It happens due to conversion of propane to CO_2 due to combustion reaction. Complete conversion of propane is observed.

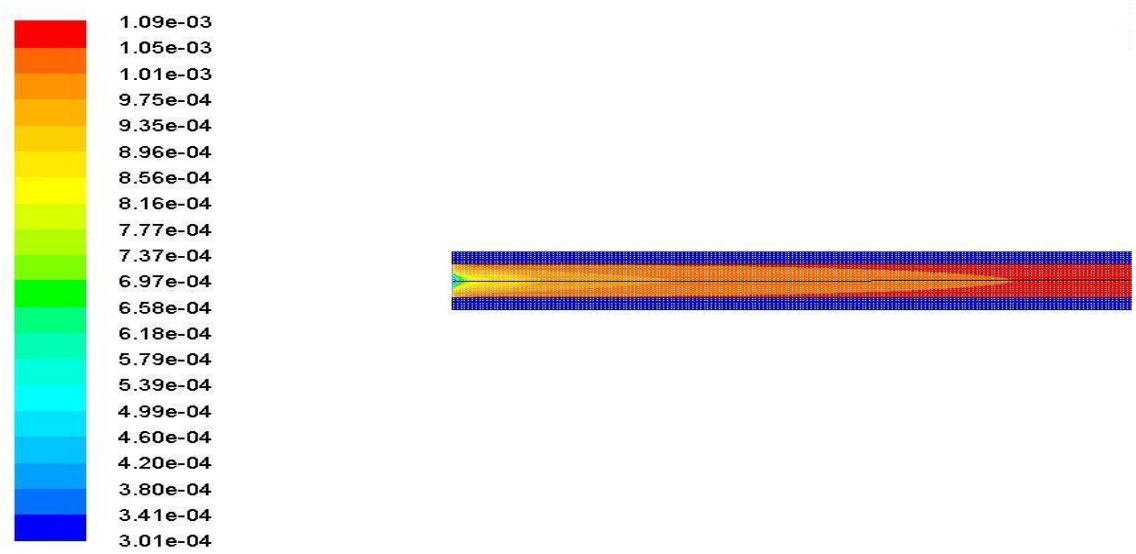

Figure 4.12: Contour plot of molar concentration of CO_2 (kmol/m^3)

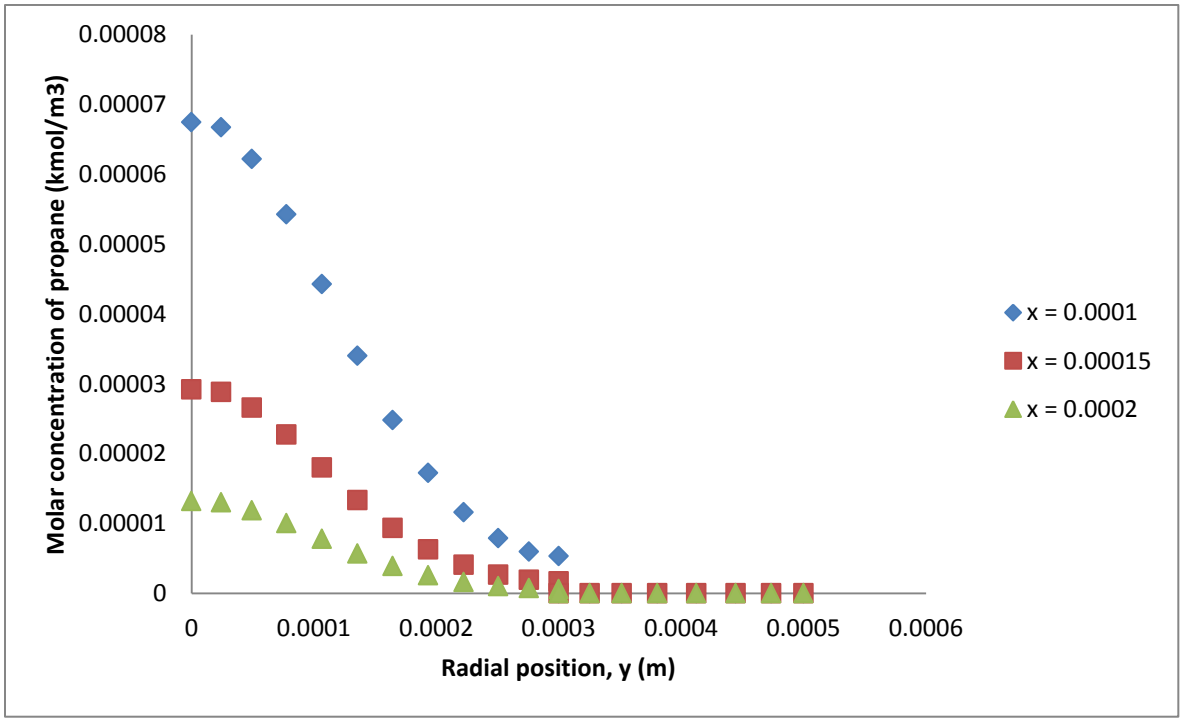

Figure 4.13: Radial concentration distribution of propane

Figure 4.13 shows the radial concentration profile of propane. It is observed that near to the center the concentration of propane is high compared to the region near to the wall. The concentration of propane at the center is mximum for radial distance 0.0001 m.

4.4 CONCLUSION

A numerical study of microburner is discussed. Combustion of propane is taken as the model reaction. Key conclusion of this chapter can be summarized as follows.

- Low wall thermal conductivity results in large axial wall-temperature gradients and high maximum temperatures and high wall thermal conductivity leads to uniform temperature profiles without hotspots.
- With increase in inlet mole fraction of propane, reaction rate also increases.
- Complete conversion of propane is observed.

CHAPTER 5

COMBUSTION OF METHANE INSIDE A MONOLITHIC REVERSE FLOW REACTOR

Chapter 5

COMBUSTION OF METHANE INSIDE A MONOLITHIC REVERSE FLOW REACTOR

Typical reactors, such as the fixed bed type often found in industry, are operated in a unidirectional manner. There is a fixed inlet and a fixed outlet. A reverse-flow reactor does not have a fixed inlet or outlet. The inlet is periodically switched between two sides of a reactor. A packed bed, monolith or other section may be used in the active section of the reactor. Monoliths are structures that contain various types of interconnected or separated channels (straight, wavy or crimped) in a single block of material (e.g. honeycombs, foams or interconnected fibers). In this chapter combustion of methane inside a monolithic reverse flow reactor is considered. A three-dimensional computational fluid dynamics model of the reactor is solved. For this case both steady and transient state simulations are considered.

5.1 PROBLEM STATEMENT

Combustion of methane over a monolith is considered. And it is assumed that kinetics should be based upon a simple single-step scheme leading directly to CO_2 and H_2O as the sole products. Table 5.1 shows the parameters for monolith packing (Gosiewski et al., 2008).

$$CH_4 + 2O_2 \rightarrow CO_2 + 2H_2O$$

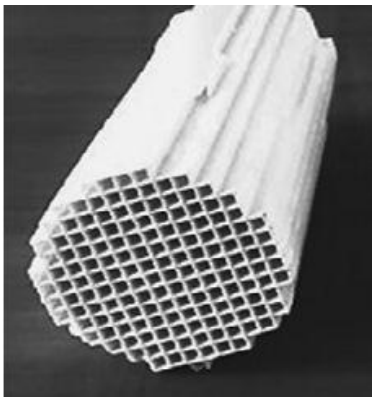

Figure 5.1: Monolith (Gosiewski et al., 2009)

Table 5.1: Parameters for monolith packing (Gosiewski et al., 2009)

Quantity	**Unit**	**Monolith**
Diameter	cm	3.9
Length	cm	40
Channel width	mm	2
Wall thickness	mm	0.5
Channels per square inch	$1/in^2$	100

5.2 FLUENT SIMULATION

The monolithic reactor considered for simulation purpose is a cylinder of diameter 0.039 m and length 1 m. The volume fraction of solid inside the reactor is 0.36.

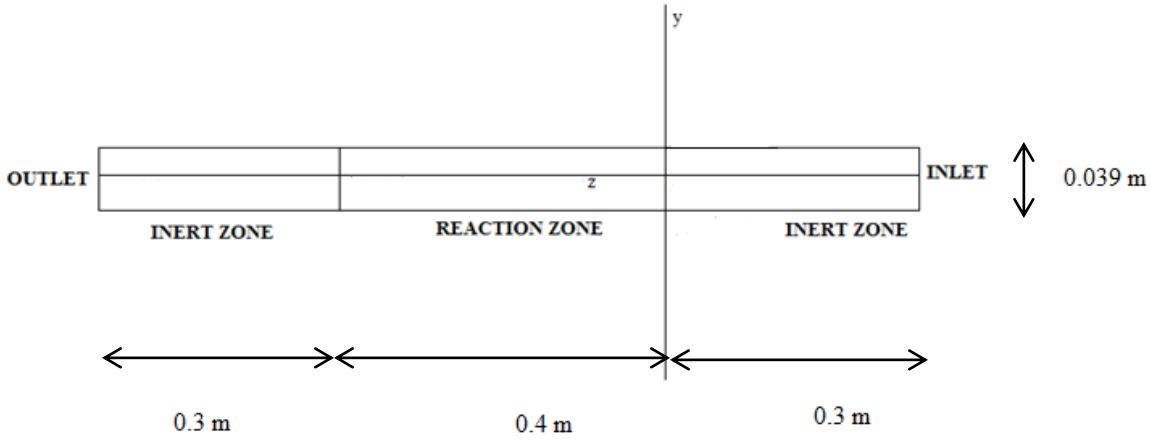

Figure 5.2: Schematic diagram of the computational domain

5.2.1 GEOMETRY AND MESH

The 3D geometry is created by using ANSYS 12 software. The geometry is created in ANSYS workbench.

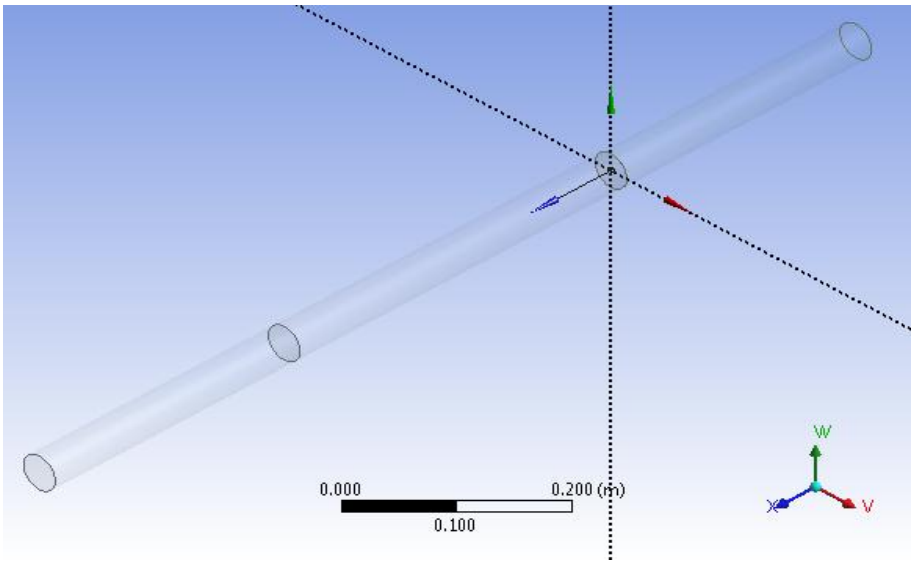

Figure 5.3: Geometry in ANSYS workbench

The geometry is meshed into smaller cells. The meshing method used is patch independent tetrahedron. The geometry is meshed into 10394 nodes and 45457 elements.

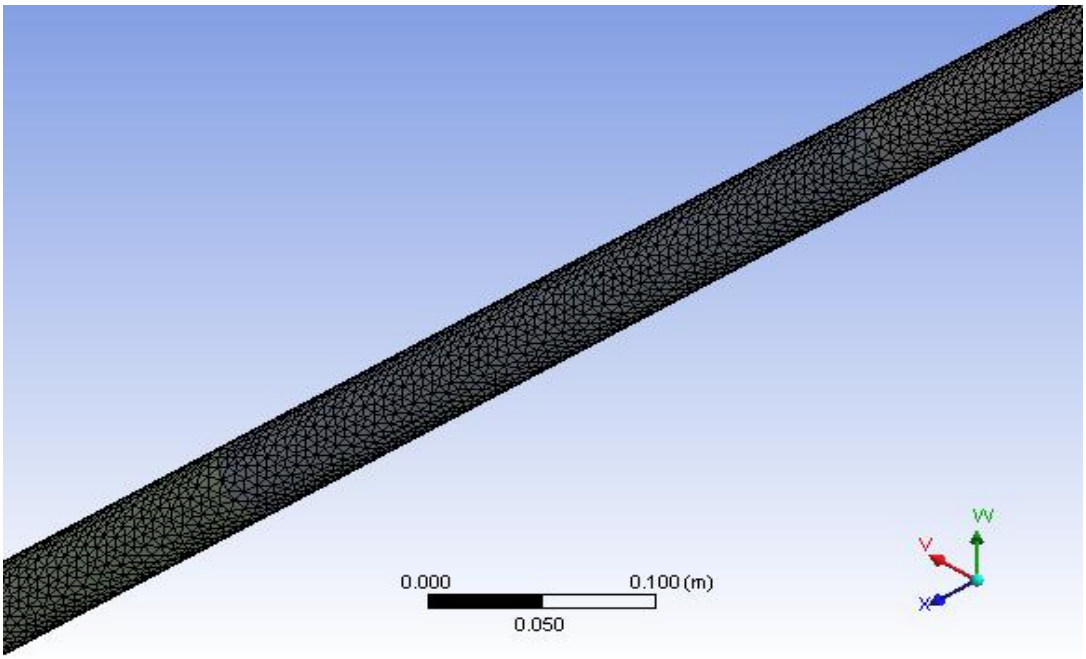

Figure 5.4: Meshing of geometry

5.2.3 BOUNDARY CONDITIONS

In order to obtain a well-posed system of equation, reasonable boundary conditions for the computational domain have to be implemented. Boundary conditions and input specifications for problem are given in Table 5.2. The wall is maintained at adiabatic condition. At the inlet, velocity of the mixture and mole fraction of the species is specified. At outlet outflow boundary condition is specified. In case of wall, no slip boundary condition is used for solid and fluid phase.

Table 5.2: Input specification

Sl No.	**Parameters**	**Value**
1	Inlet flow velocity	0.1163 m/s
2	Inlet mole fraction of methane	1.8%
3	Inlet mole fraction of methane	98.2%
4	Inlet temperature	300K
5	Pre-exponential factor	6.861×10^{6} $mol^{0.06}m^{-0.18}s^{-1}$
6	Activation energy	130.622 KJ/mol^{-1}
7	Reaction order	0.94

5.2.4 SOLUTION TECHNIQUES

In Fluent, solver is set as segregated which solves the equation individually. Steady state simulation has been formulated. Here pressure based solver is used. Species transport model is used. Eulerian multi-fluid model is adopted where liquid and solid phases are all treated as continua, inter- penetrating and interacting with each other everywhere in the computational domain. Mehane-oxygen mixture is treated as the primary phase. The finite rate model is considered. Finite rate model is used to predict the reaction rate. The discretization scheme for momentum, energy, volume fraction and all has been taken as first order upwind for solid and gas phase. The following under relaxation factors have been used for different flow quantities: pressure: 0.1, density: 1, body forces: 1, momentum: 0.1, volume fraction: 0.1, granular temperature: 0.2, energy: 0.1 and species: 0.1.The convergence criterion for continuity, velocity and species is 0.001.The initial guess value of wall temperature of reaction zone considered is

1173 K. Under adiabatic condition low temperature convergence was achieved. Hence no reaction was taking place. So the wall temperature is initialized to a higher value. After initialization, patching of solid is done.

5.3 RESULTS AND DISCUSSION

5.3.1 STEADY STATE SIMULATION

This section describes the steady state simulation results. The steady state characteristics of temperature distribution and concentration distribution along the axial and radial distance are studied. The effect of various parameters such as inlet mole fraction of methane, mass diffusivity and inlet temperature on steady state temperature distribution is also described. The steady state simulation result was used as the basis for transient simulation. When the model was simulated directly using the transient condition only, low temperature convergence was observed. Hence no reaction was taking place inside the reactor. Hence the model was first solved in steady state. The result of steady state solution was used as the initial condition for transient state simulation.

The axial temperature distribution has been shown in the Fig. 5.5 for the inlet velocity 0.1163 m/s and inlet temperature 300K. It is observed that temperature varies with axial length. At first the temperature increases, reaches the maximum and then decreases. The temperature rise occurs due to the exothermicity of the combustion reaction. Fig. 5.6 shows the axial concentration distribution of methane. The molar concentration of methane is decreasing with axial length. The variation of concentration of methane can clearly be visualized in the Fig. 5.7 which depicts the contour plot of mass fraction of methane.

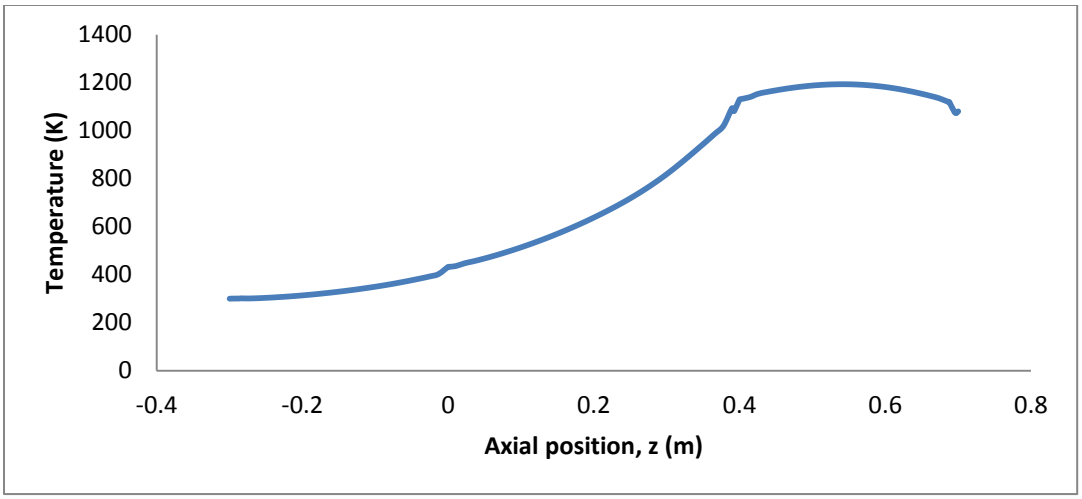

Figure 5.5: Steady state axial temperature distribution at the centerline of the reactor

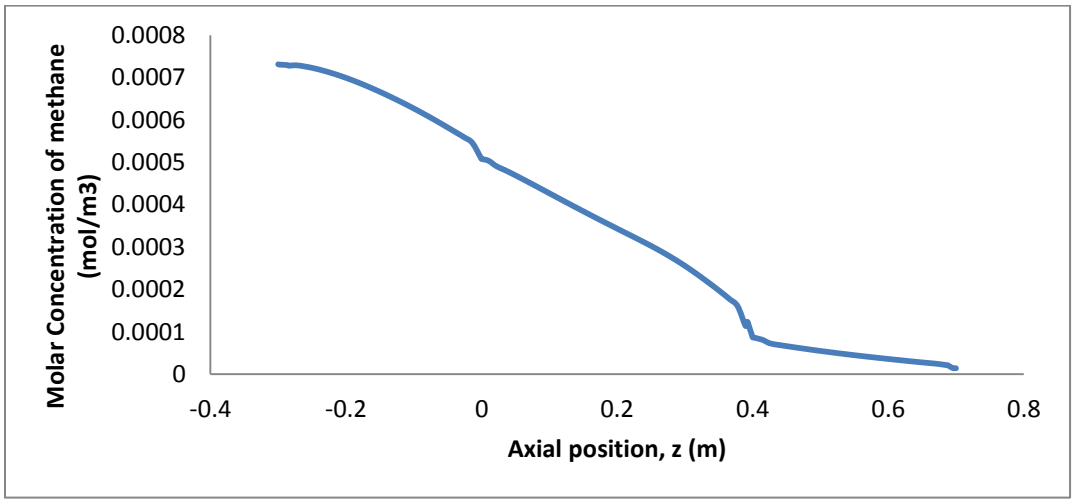

Figure 5.6: Steady state axial concentration profile of methane

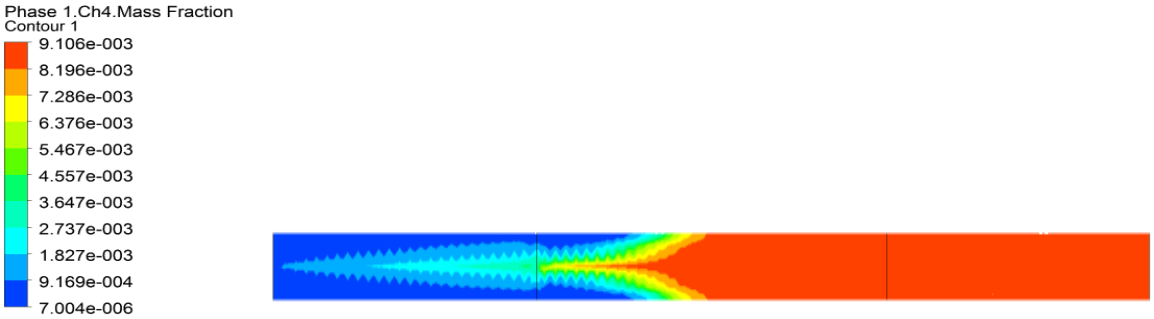

Figure 5.7: Contour plot of mass fraction of methane

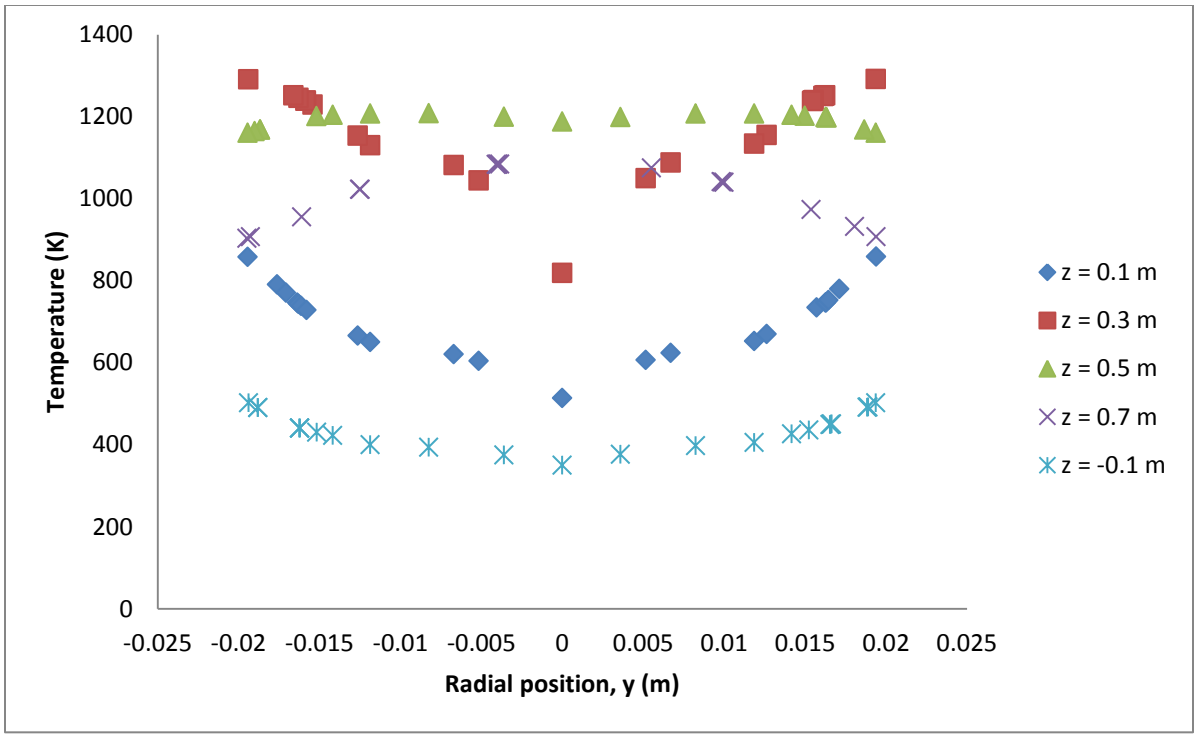

Figure 5.8: Steady state radial temperature distribution at a particular axial distance, z.

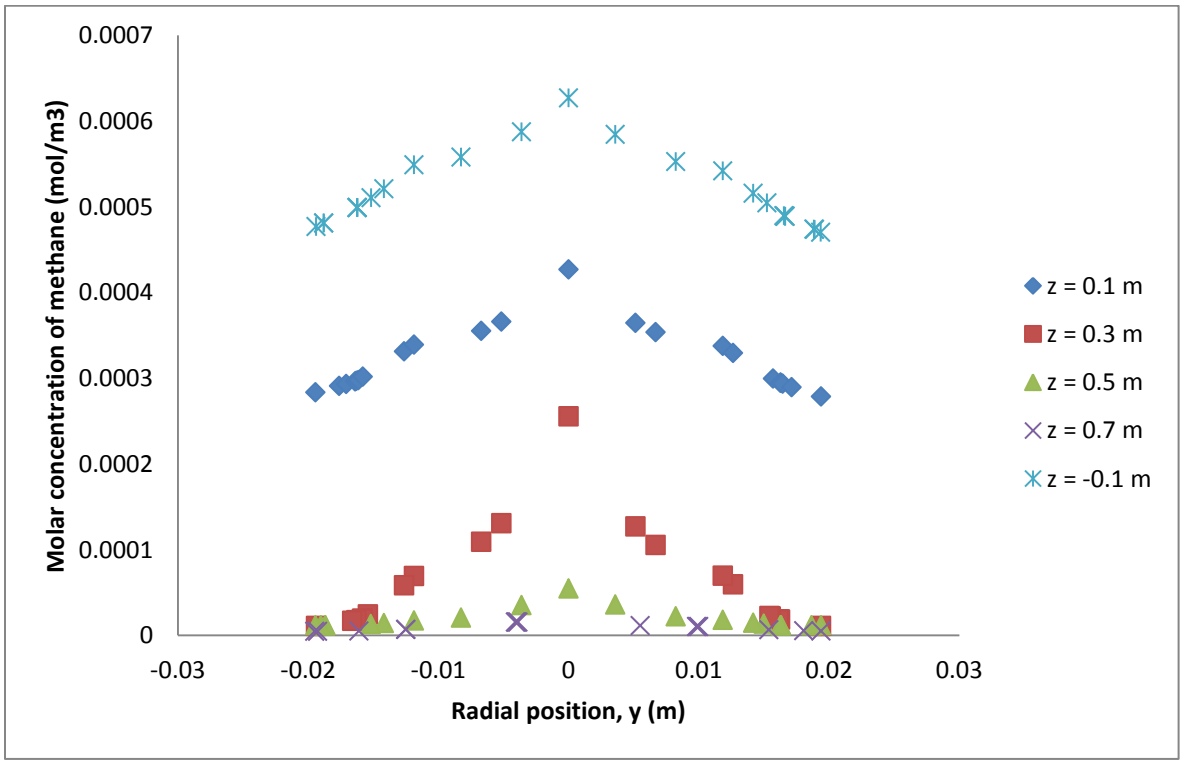

Figure 5.9: Steady state radial concentration profile of methane at a particular axial distance, z.

Fig. 5.8 shows the radial temperature distribution at different axial position. It is observed that the temperature of the fluid near to the wall is maximum compared to the center of the reactor except for axial position 0.5 m and 0.7 m. in this two radial position the temperature near the wall is less compared to the center. As the wall of the reaction zone is initialized to a higher temperature, the reaction first starts near the wall of reaction zone then it proceeds toward the center. Due to larger extent of reaction, wall temperature is more nearer to the inlet of the burner. But at the axial distance away from the inlet, more combustion happens around the centerline and hence centerline temperature is more than wall. The radial concentration of methane at different position is shown in Fig. 5.9. The concentration of methane near the wall is found less compared to the center. The relative higher level of methane concentration at the center nearer to the inlet of the burner is observed than away from the inlet position. It happens due to larger extent of reaction nearer to the wall. It is also observed that at any radial position, methane concentration decreases with axial distance which occurs due to conversion of methane to carbon dioxide.

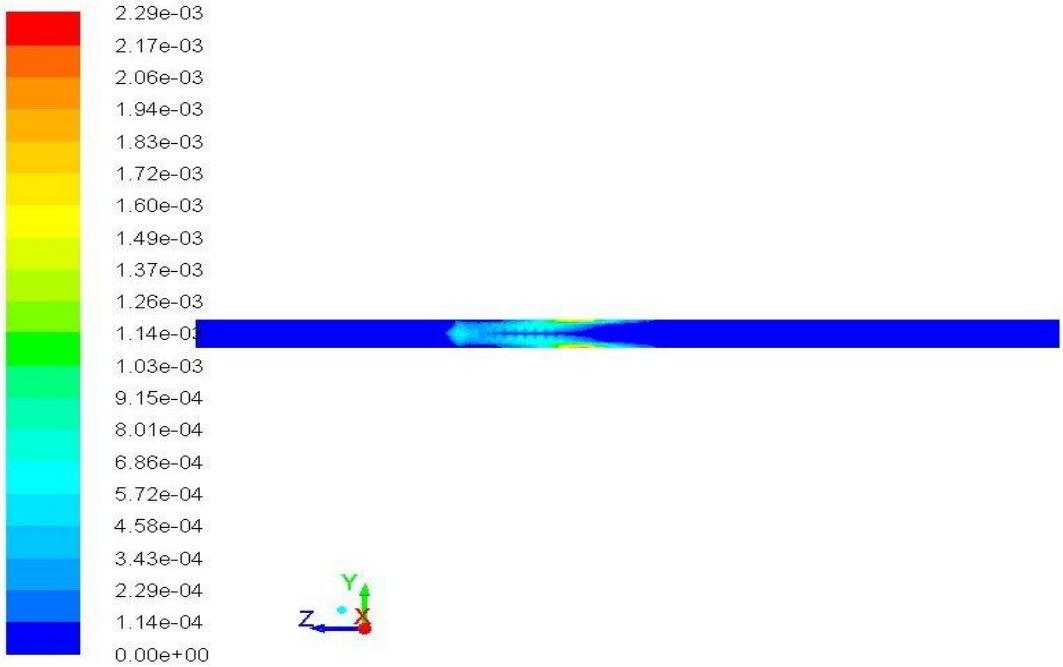

Figure 5.10: Contour plot of kinetic reaction rate (kmol/m^3-s)

Fig. 5.10 shows the contour plot of reaction rate. Here for modeling reaction, finite rate model is considered. The reaction starts near the wall and then proceeds towards the center.

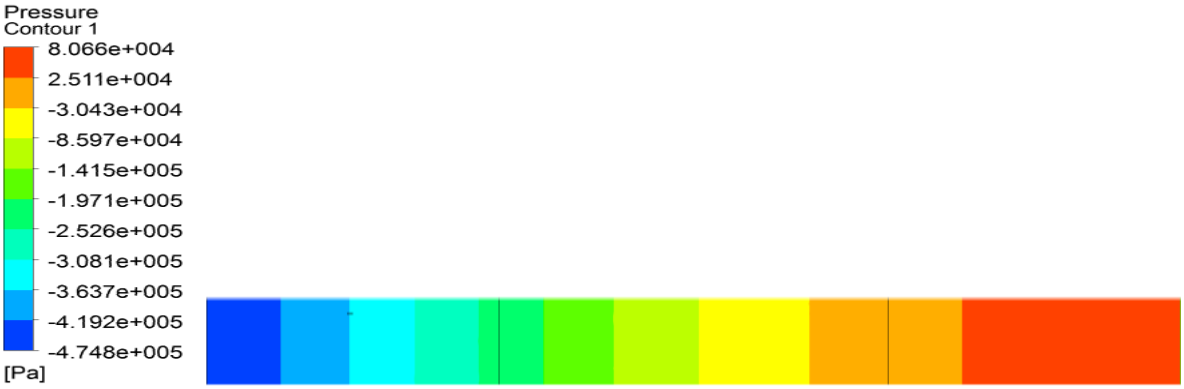

Figure 5.11: Contour of pressure (Pa)

The pressure distribution in Fig. 5.11 shows a linear variation of pressure with axial distance and pressure distribution is also found independent of radial position.

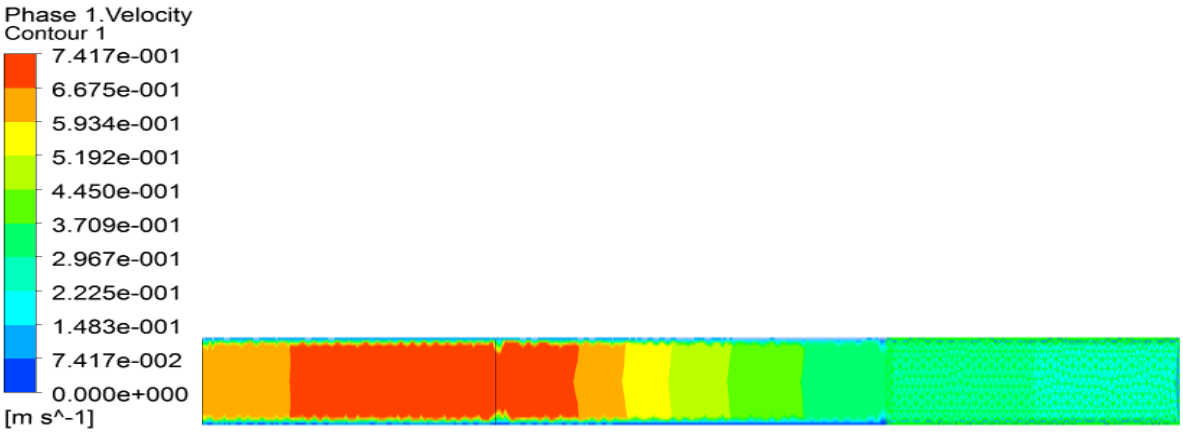

Figure 5.12: contour plot of velocity of gas (m/s)

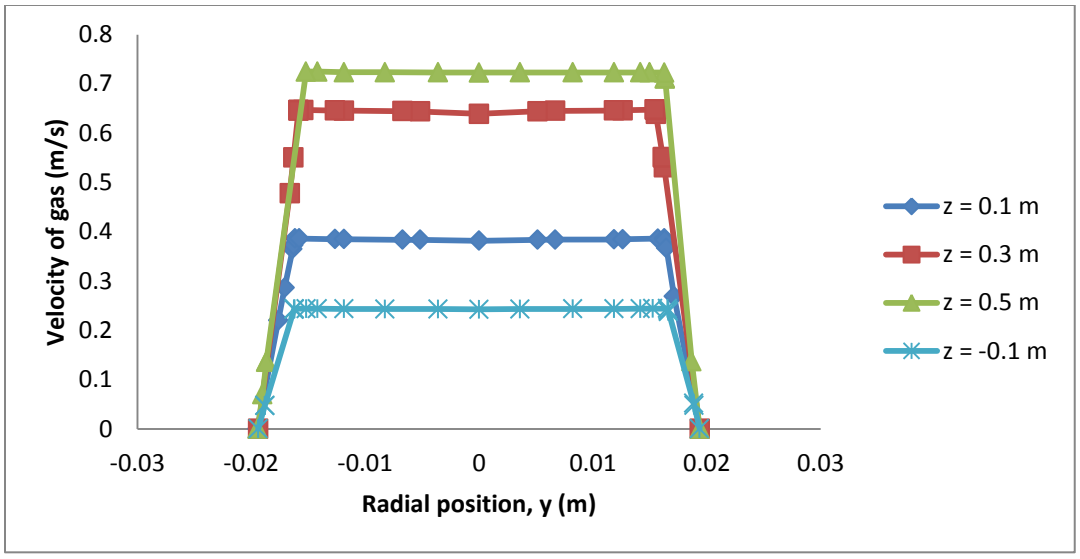

Figure 5.13: Radial velocity profile of gas

The velocity distribution of gas inside the reverse flow reactor is clearly visualized in the contour plot of velocity shown in Fig. 5.12. The velocity at different radial position is displayed in Fig. 5.13. The velocity of the gas is zero exactly at the wall. A flat velocity profile is observed. Hence flow behaviour is almost plug flow type.

The effects of parameters like inlet temperature, mass diffusivity, and wall heat transfer coefficient and inlet mole fraction of methane on the combustion behavior are studied.

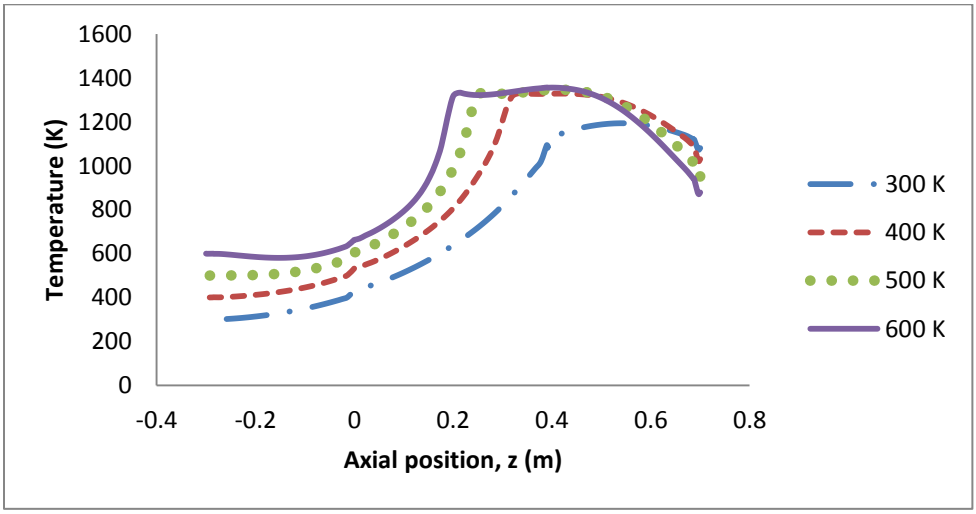

Figure 5.14: Axial temperature profile for different inlet temperature

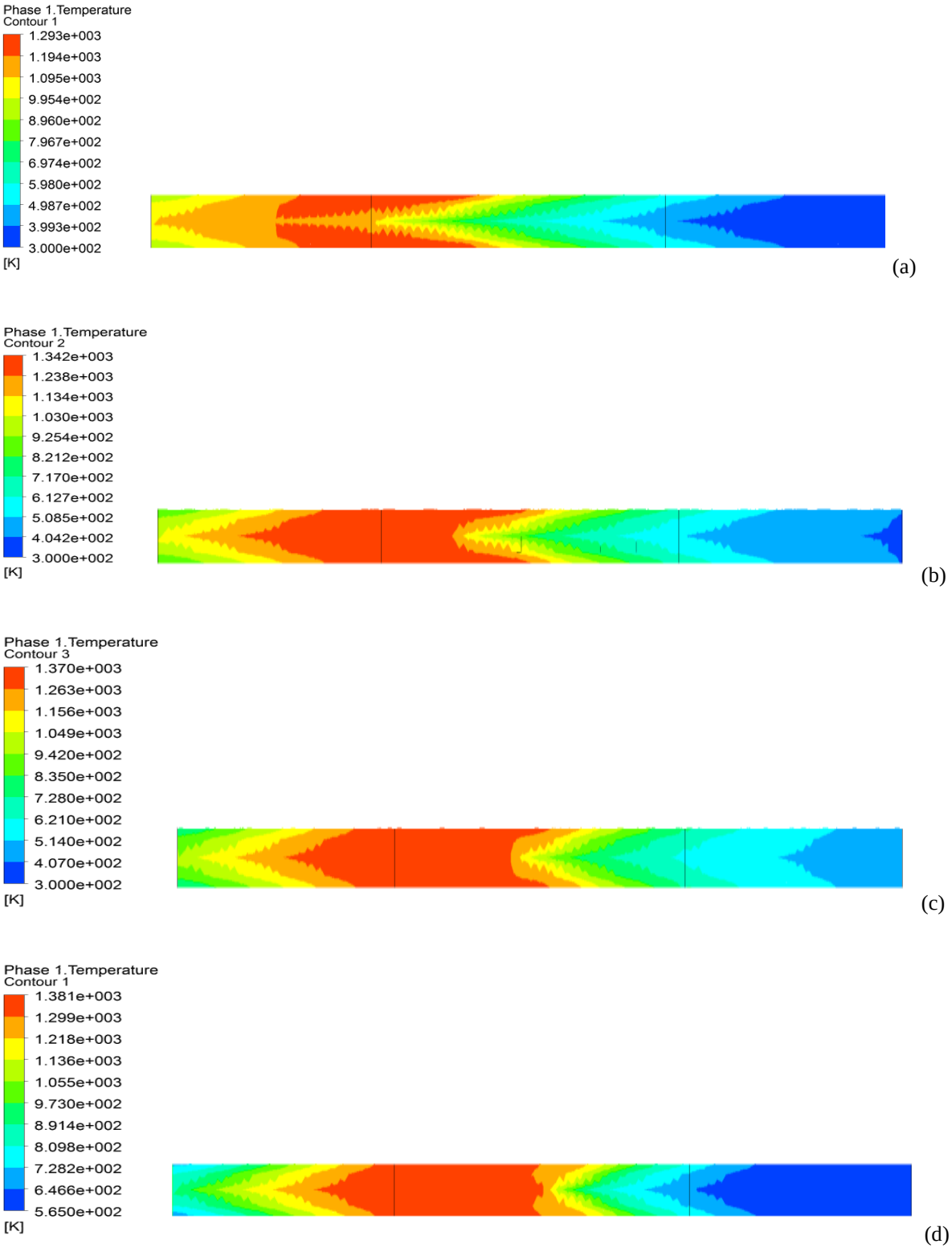

Figure 5.15: Contour plots of temperature of the fluid (phase 1) inside the reactor at different inlet temperature (a) 300K; (b) 400K; (c)-500K; (d) 600K

It is observed in Fig. 5.14 and 5.15 that gas mixture temperature increases with increase in inlet temperature. Increase in inlet temperature, increases the reaction rate and hence higher conversion is achieved. Due to increase in reaction rate, temperature of the fluid also increases. At any particular inlet temperature, it is also found that temperature increases till halfway of the reaction zone and then it decreases with increase in axial distance even in reaction zone. As the inlet temperature increases, the maximum temperature is found at larger axial distance. Due to appearance of the early maximum temperature, more amount of heat is absorbed by the solid in the packed bed at larger inlet temperature, and hence the outlet temperature of fluid is less for larger inlet temperature.

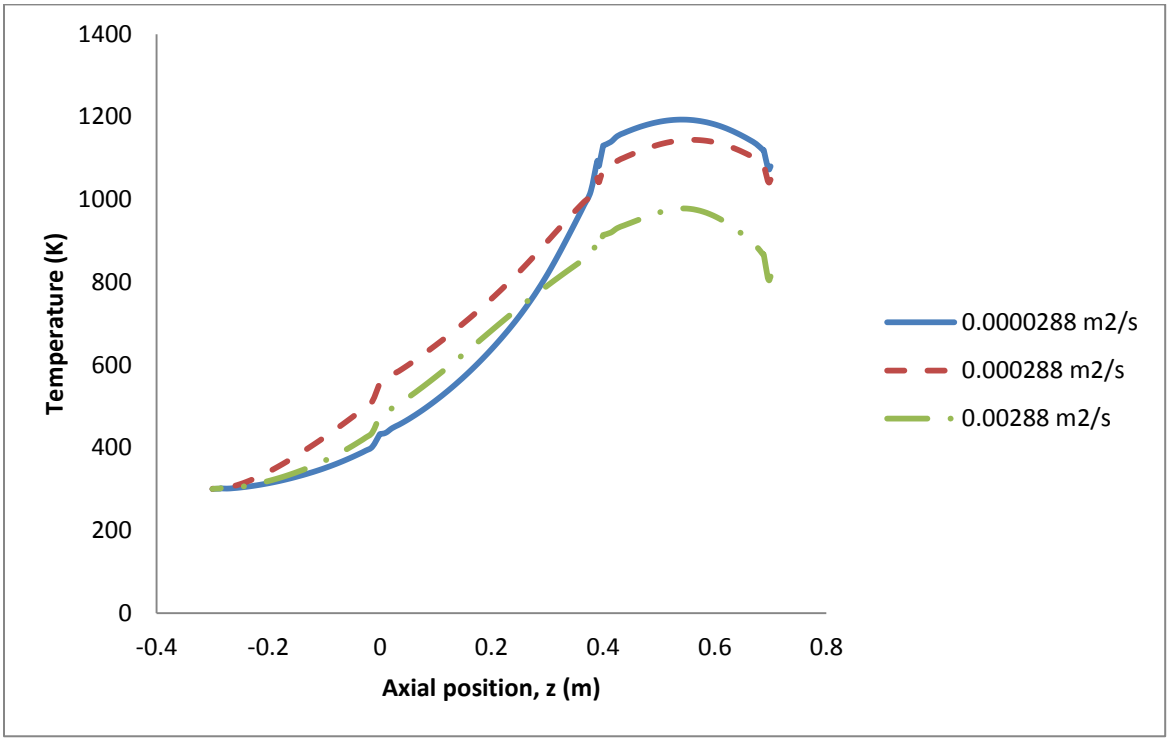

Figure 5.16: Axial temperature profile for different mass diffusivity

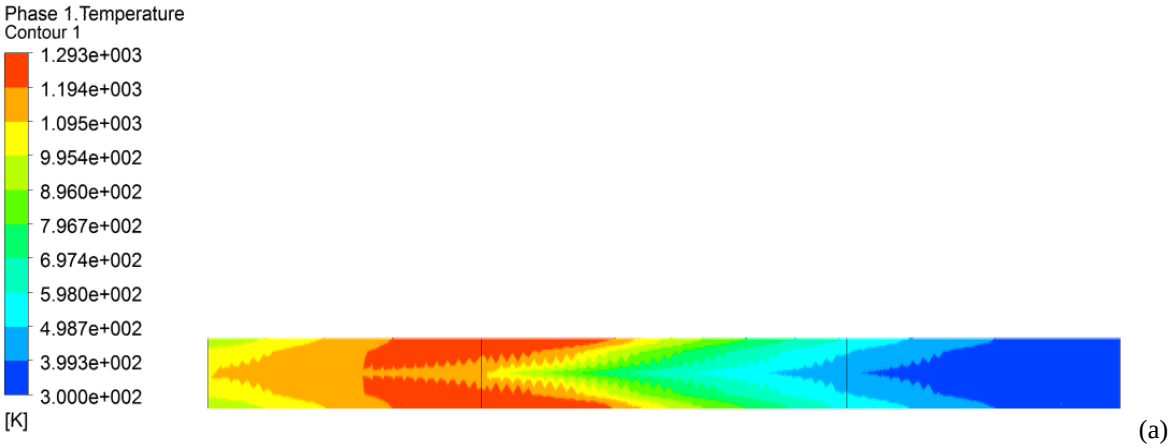

(a)

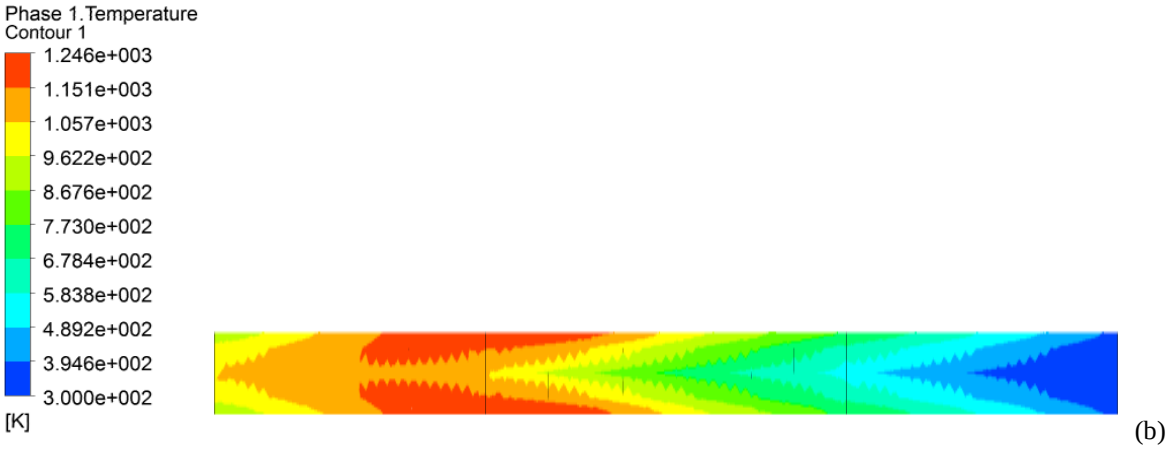

(b)

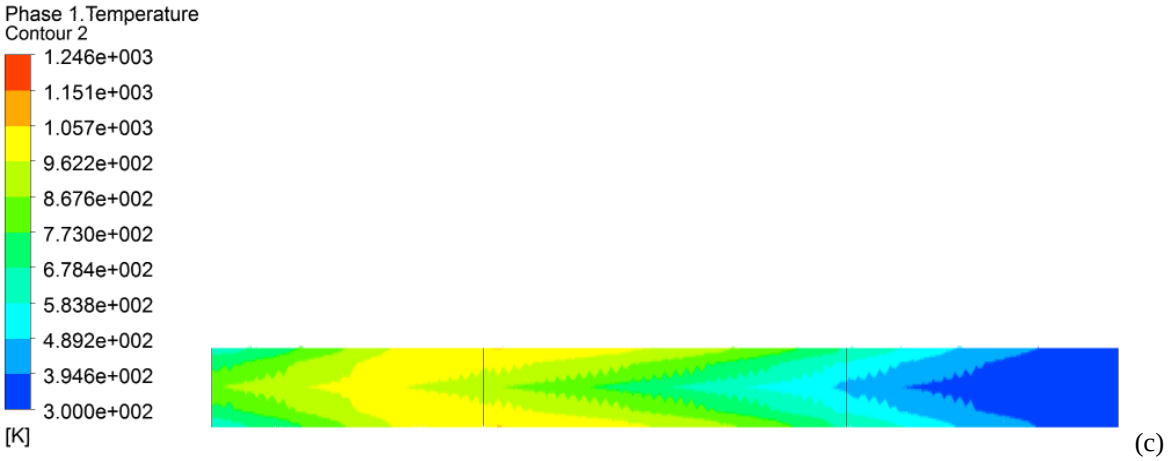

(c)

Figure 5.17: Contour plots of temperature of the fluid inside the reactor at different mass diffusivity (a) 0.0000288 m^2/s, (b) 0.000288 m^2/s; (c) 0.00288 m^2/s

From Fig. 5.16 and Fig. 5.17, it is observed that with increase in mass diffusivity of methane-oxygen mixture, maximum temperature of the fluid decreases.

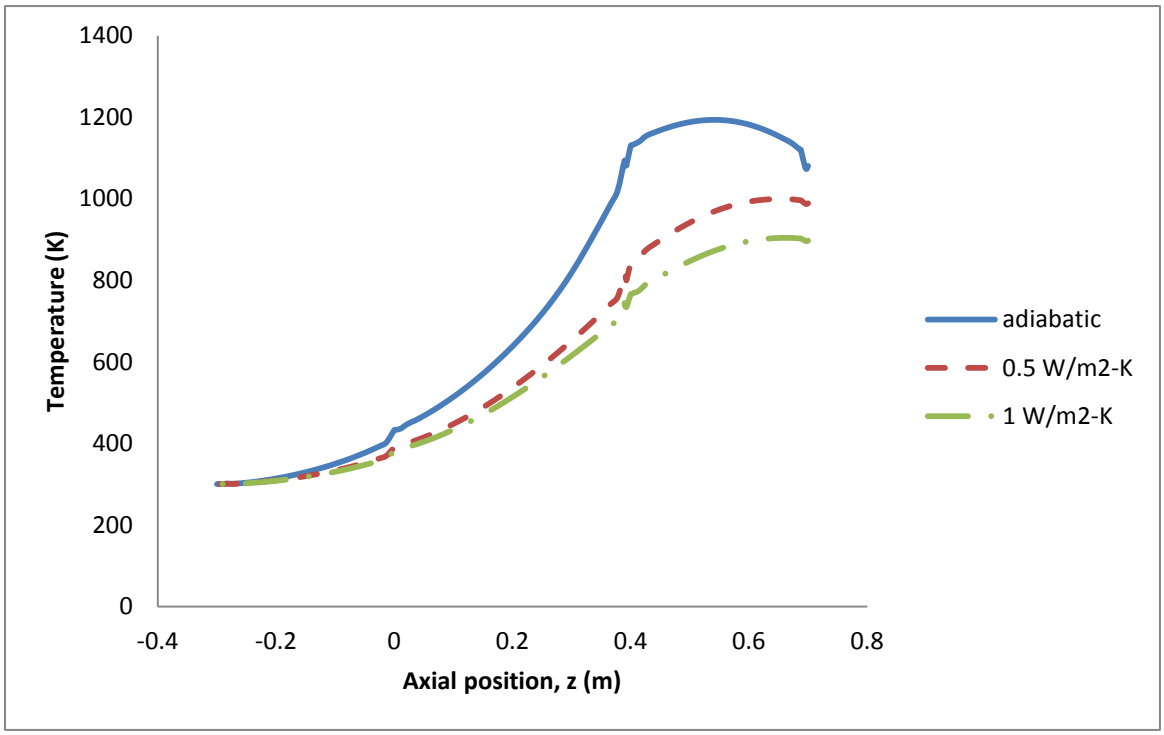

Figure 5.18: Axial temperature profile for different wall heat transfer coefficient

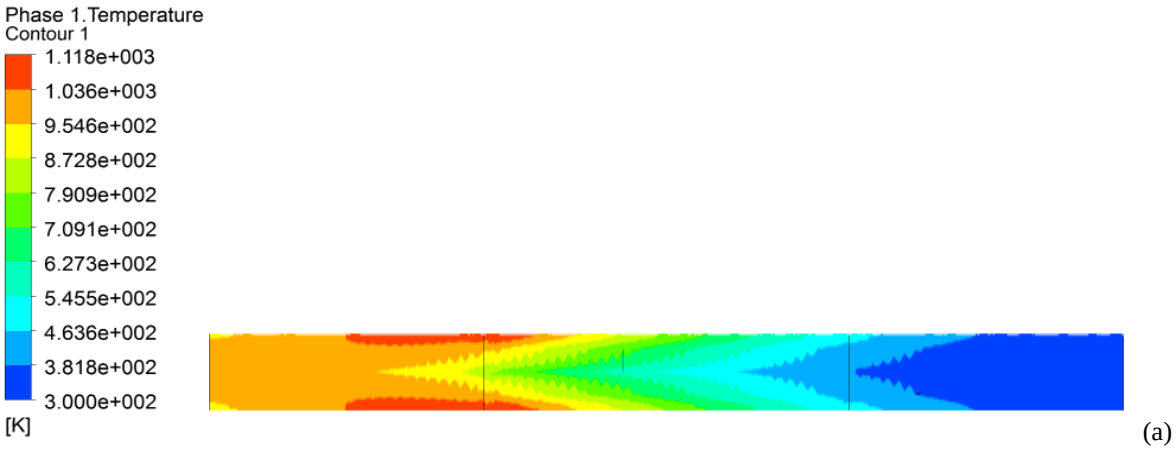

(a)

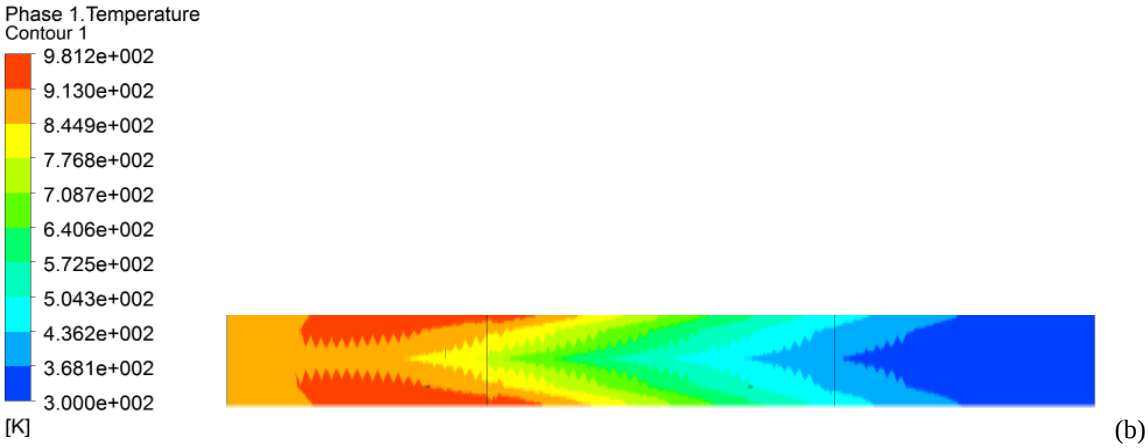

Figure 5.19: Contour plots of temperature of the fluid inside the reactor at wall heat transfer coefficient (a)-0.5 W/m2-K; (b)- 1W/m2-K

From Fig. 5.18 and Fig. 5.19, it is observed that with increase in wall heat transfer coefficient, maximum temperature of the fluid decreases. The ambient temperature considered is 300 K. With increase in wall heat transfer coefficient, heat loss to the surrounding increases and hence reaction rate decreases which leads to decrease in temperature of the fluid.

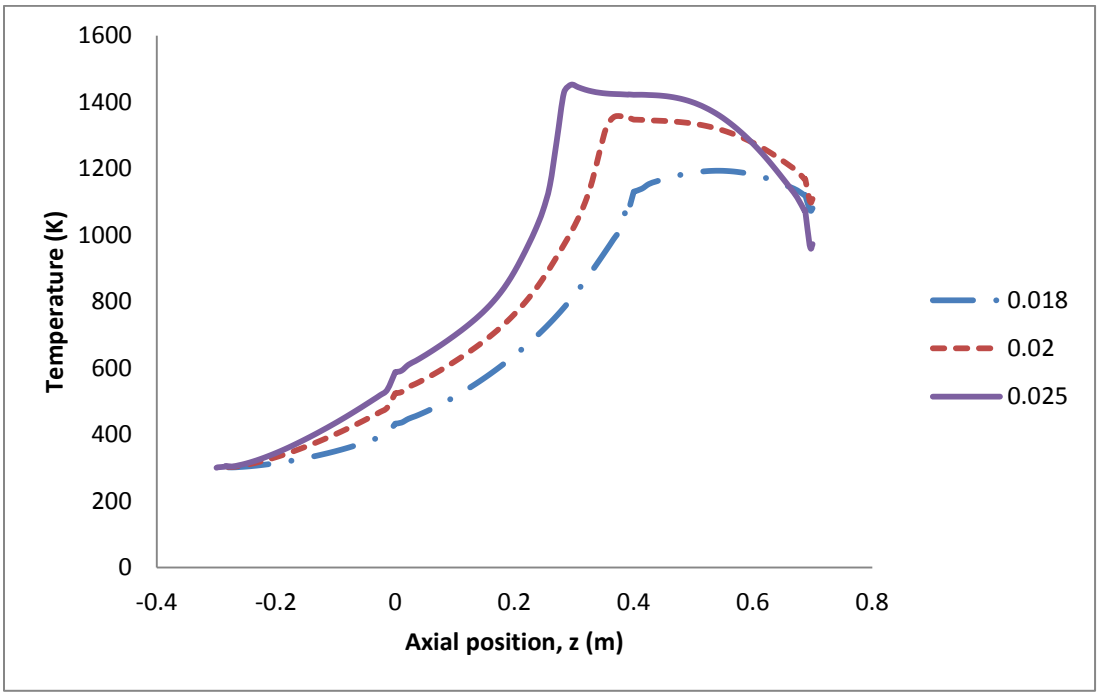

Figure 5.20: Axial temperature profile for different inlet methane concentration (mole fraction)

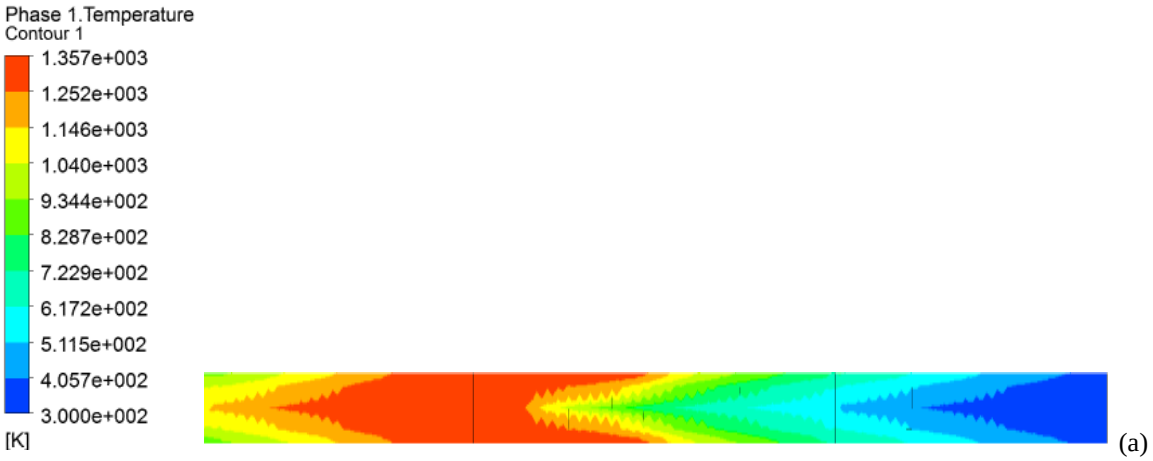

Figure 5.21: Contour plots of temperature of the fluid inside the reactor at different inlet methane mole fraction (a)-0.02; (b)- 0.025

From Fig. 5.20 and Fig. 5.21, it is observed that with increase in inlet methane concentration the maximum temperature of the gas also increases. The reaction rate expression depends on the concentration of the methane. Hence increase in inlet molar concentration of methane leads to increase in rate of reaction which in turn increases the temperature of the gas.

5.3.2 TRANSIENT SIMULATION

After achieving the steady state value, the inlet and outlet boundary conditions are reversed and without initializing the solution, the simulations are again carried out for transient case. The simulations are carried up to t = 1020 s and the flow direction is reversed after every 30 s.

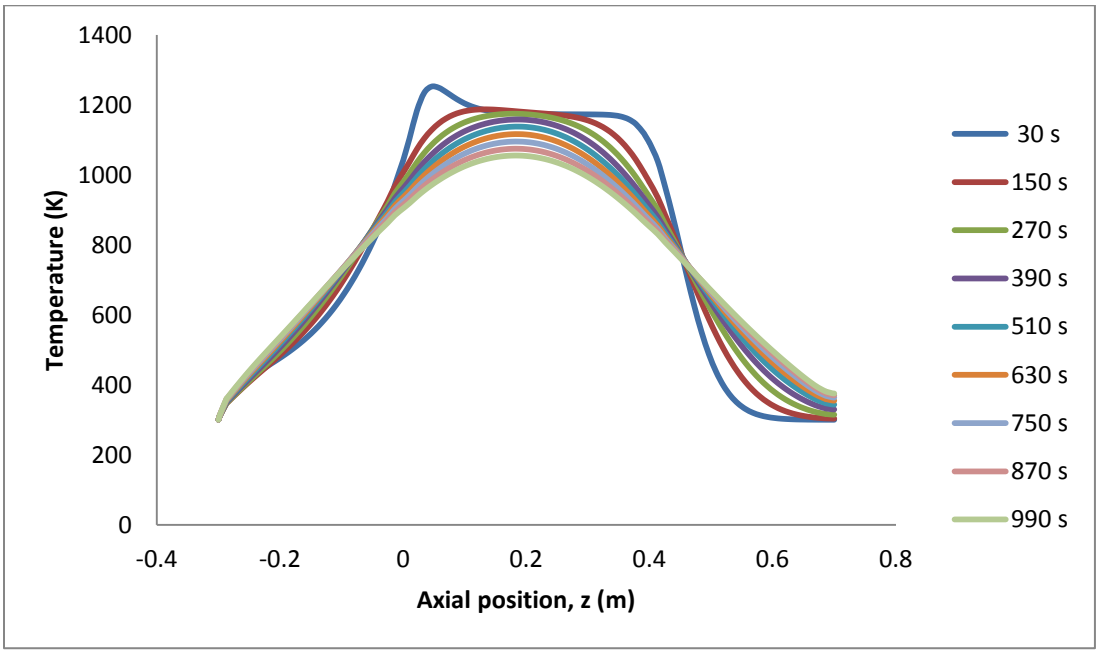

Figure 5.22: Axial temperature profile

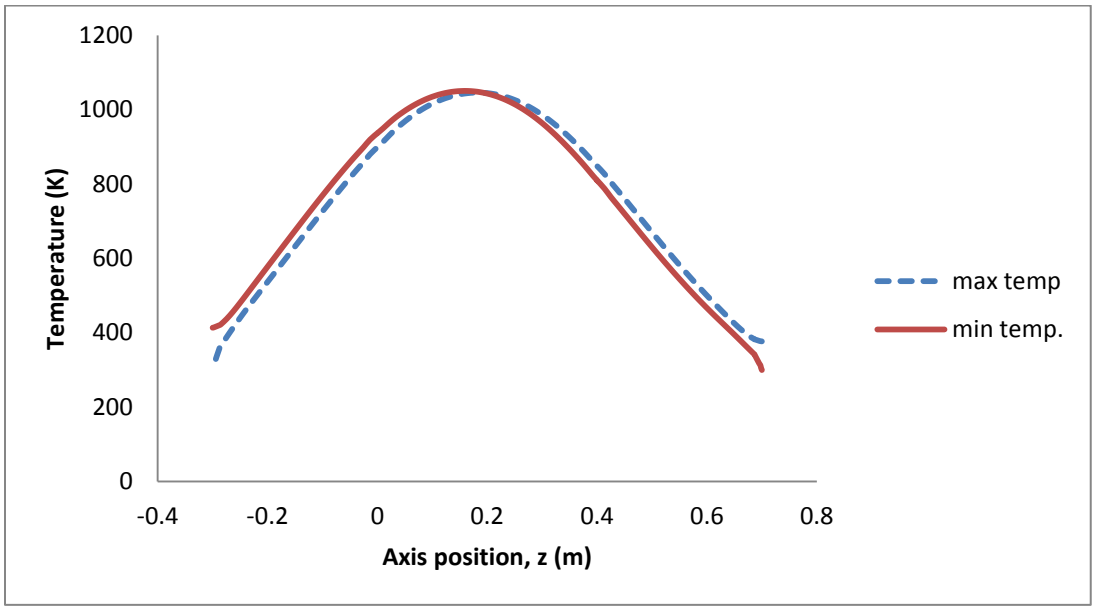

Figure 5.23: Axial maximum and minimum temperature profile

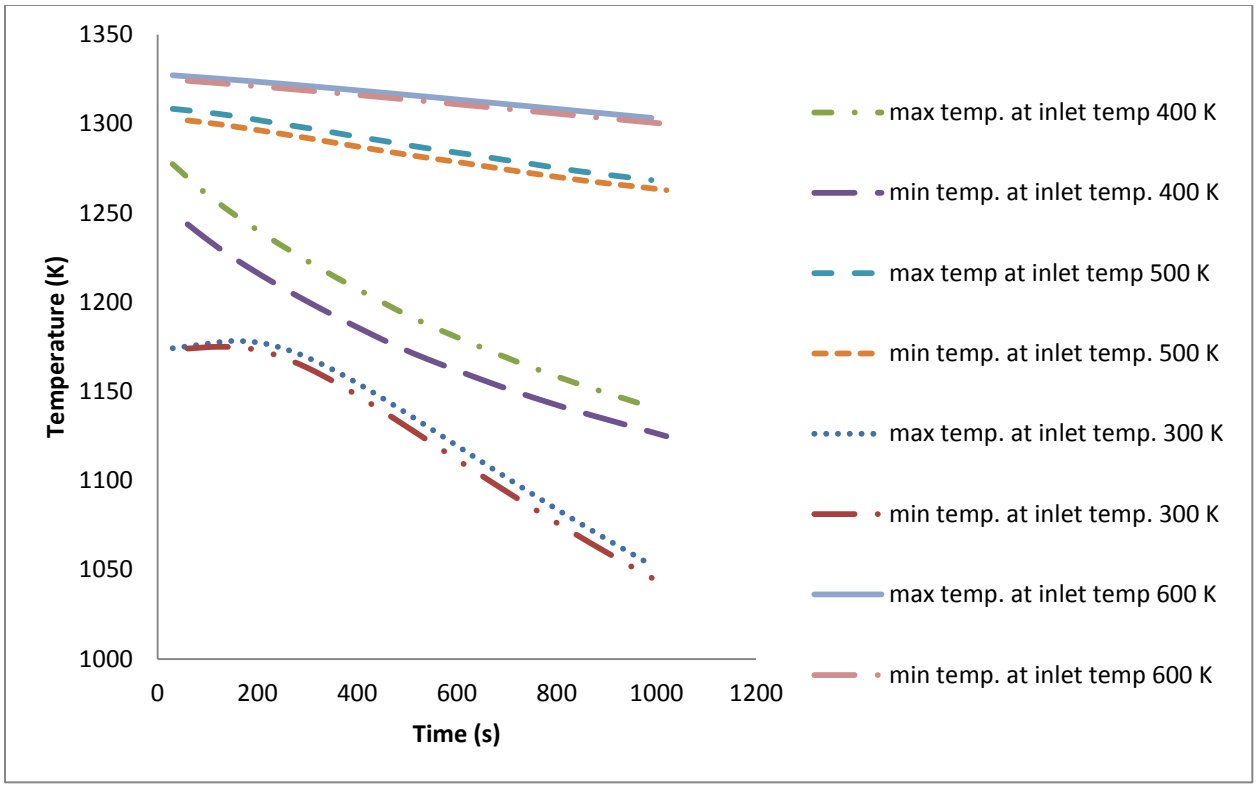

Figure 5.24: Temperature at the center of the reactor (0, 0, 0.2) for different inlet temperature

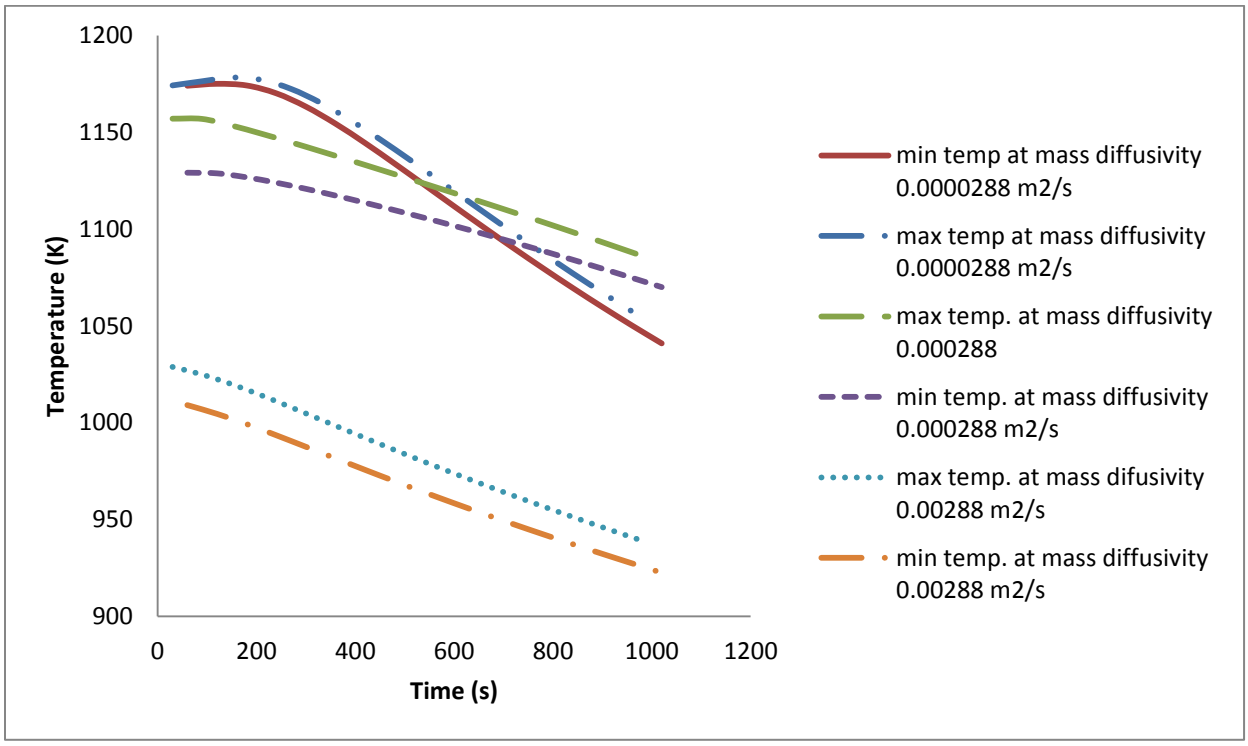

Figure 5.25: Temperature at the center of the reactor (0, 0, 0.2) for different mass diffusivity

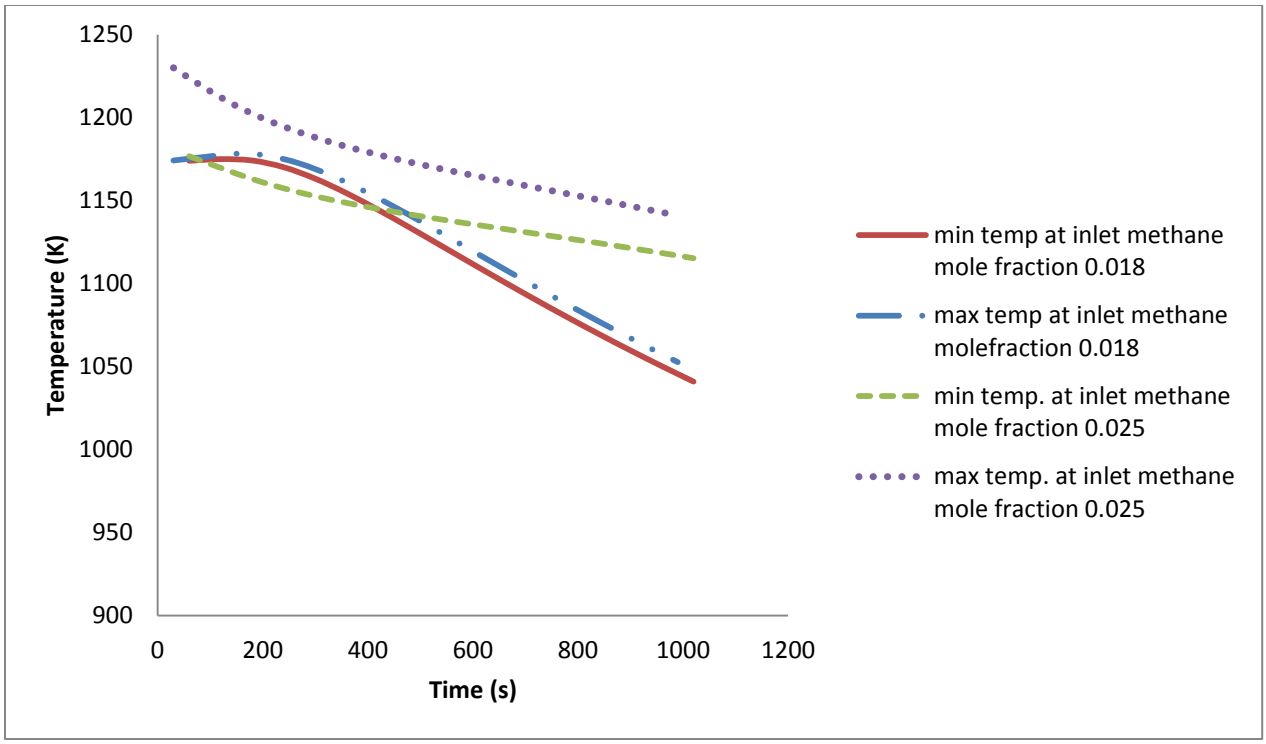

Figure 5.26: Temperature at the center of the reactor (0, 0, 0.2) for different inlet methane mole fraction

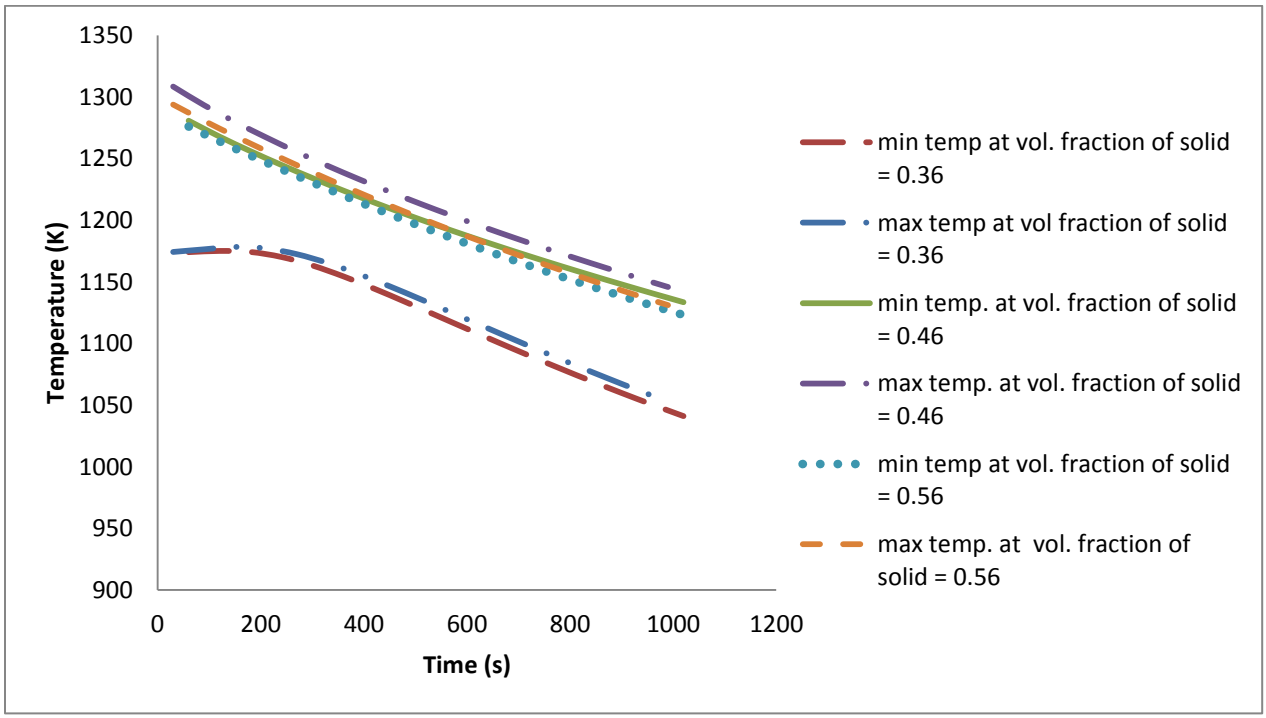

Figure 5.27: Temperature at the center of the reactor (0, 0, 0.2) for volume fraction of solid

In case of a reverse flow reactor, a full reversal cycle consist of two half cycles. In the first half cycle the reaction mixture in the reactor flows in one direction, whereas in the second half cycle the flow is in the opposite direction. The moment at which the flow direction returns to the initial one is marked as the end of one full reversal cycle. For the problem considered in this chapter, the half cycle period is 30 s. The temperature of the gas inside the reverse-flow reactor fluctuate in every cycle of reversal. Thus, during the simulation both minimum and maximum temperatures are recorded. Fig. 5.22 shows the centerline temperature variation with time. It is observed that the maximum temperature of the gas decreases with time for specified inlet specifications.

In this report effect of various parameters on the temperature of the gas at center of the reactor are studied. Fig. 5.24 shows the effect of inlet temperature on the temperature of the gas at the center of the reactor i.e. (0, 0, 0.2). With increase in inlet temperature, the reactants react at a higher temperature and reaction rate increases owing to which maximum and minimum temperature of the gas also increases at a particular time. But as the time passes, the value of maximum and minimum temperature decreases. In addition to the above, it is also observed that the difference between maximum temperature and minimum temperature is more in case of inlet temperature 400 K and for inlet temperature 600 K the difference is negligible.

Fig. 5.25 shows the effect of mass diffusivity on the temperature of the gas at the center of the reactor. The temperature of the gas at the center of the reactor increases with decrease in mass diffusivity. This increase is due to the increased rate of combustion near the center of the reactor. It also observed that after a certain period of time, the temperature in case of mass diffusivity 0.0000288 m^2/s is less compared to the same in case of mass diffusivity 0.000288 m^2/s.

The effect of inlet methane concentration on temperature of the gas at the center of reactor is shown in Fig. 5.26. There is an increase in maximum temperature of the gas for a particular time with increase in inlet mole fraction of methane. The reaction rate increases with increase in inlet methane concentration. In this problem single step kinetic model is used and the reaction rate expression consists of methane concentration term and oxygen concentration term is neglected as it is present in excess quantity in the inlet feed.

Effect of volume fraction of solid on transient temperature profile is also studied. It is shown in Fig. 5.27. It is observed that there is a vast increase in maximum and minimum temperature of the gas with increase in volume fraction of solid from 0.36 to 0.46. But the increase ceases with further increase in volume fraction of solid.

The simulated results are compared with the experimental results. Comparison of experimental maximum and minimum temperature (Gosiewski et al., 2008) with present CFD results is shown in the Fig. 5.28 and Fig. 5.29.

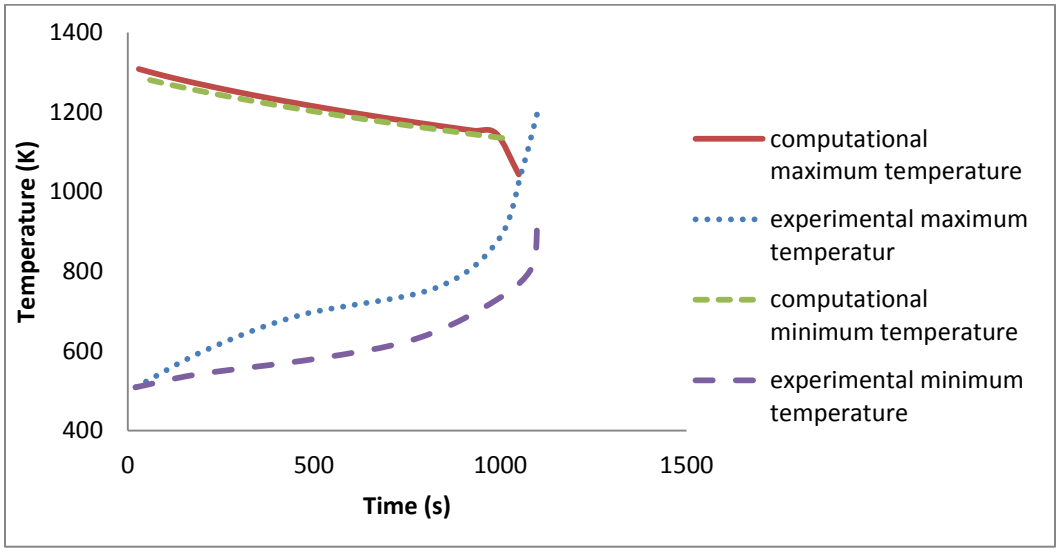

Figure 5.28: Maximum and minimum temperature of the gas at center of the reactor (0, 0, 0.2)

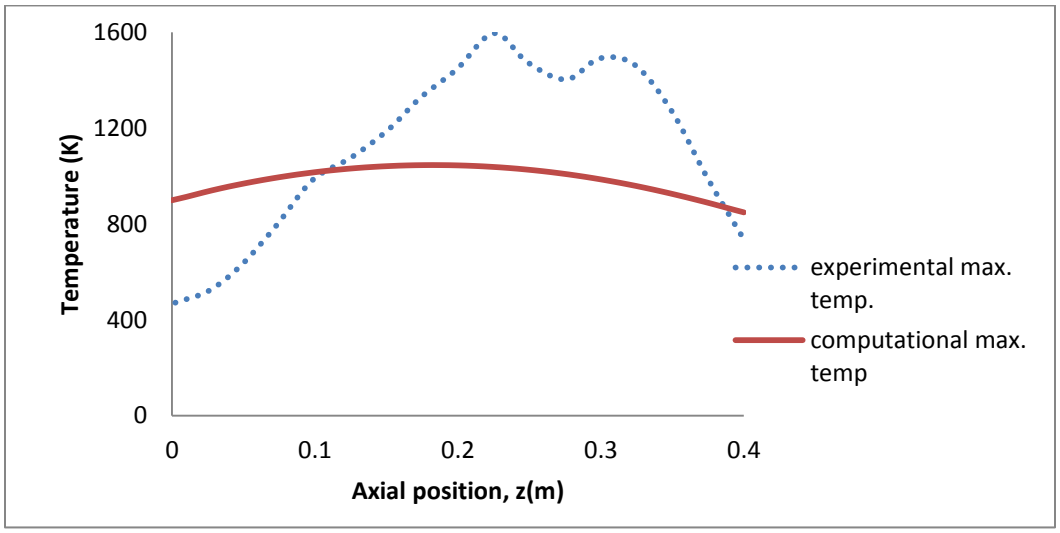

Figure 5.29: Axial maximum temperature of the gas

It is observed from the figures that the CFD results are not in good agreement with the experimental results. This is because in the present study under transient condition low temperature convergence was observed. Hence no reaction was taking place. Due to this reason the model was first solved in steady state condition. After obtaining the steady state value the flow direction was reversed i.e. the inlet and outlet boundary conditions were reversed and without initializing the solution the simulations were carried for a specified time.

5.4 CONCLUSION

CFD analysis of reverse flow reactor is carried out using both steady state and transient simulations. It is observed that

- CFD results are able to capture the trend of experimental results but magnitude wise some disagreement was observed.
- The temperature of the gas increases with axial length, reaches maximum and then decreases. With increase in inlet temperature, maximum temperature of the fluid increases.
- The temperature peak decreases with increase in mass diffusivity of the mixture and wall heat transfer coefficient.
- The reaction starts near the wall and then proceeds towards the center.

CHAPTER 6

CONCLUSION

Chapter 6

CONCLUSION

In this chapter major conclusions of the present study work are summarized. Microchannels provide an opportunity to integrate heat transfer, fluid mixing and chemical reaction in the same unit and thereby reducing the number of other components. Besides, this leads to accelerated reaction rate, reduced residence time and improved selectivity and yield as compared to conventional reactor set up. In this report main emphasis is given on reverse flow reactor. Both steady and transient state models were simulated using ANSYS Fluent 12.0. The effect of inlet methane mole fraction, inlet temperature and mixture diffusivity on temperature profile of the reactor was found in both the models.

The following conclusions are drawn for reverse flow reactor

- With increase in inlet temperature, maximum temperature of the fluid increases.
- The temperature peak decreases with increase in mass diffusivity of the mixture and wall heat transfer coefficient.
- With increase in inlet mole fraction of methane, maximum temperature of the fluid increases.
- The reaction starts near the wall and then proceeds towards the center.

REFERENCES

1. Abbasi, R., Wu, L., Wanke, S.E., Hayes, R.E., ‘‘Kinetics of methane combustion over Pt and Pt–Pd catalysts’’, Chemical Engineering Research and Design, 2012, 1-13.
2. Adeosun, J.T., Lawal, A., ‘‘Numerical and experimental studies of mixing characteristics in a T-junction microchannel u sing residence-time distribution’’, Chemical Engineering Science, 2009, 2422 – 2432.
3. ANSYS Fluent 12.0 Theory Guide, April, (2009).
4. Annaland, M.S., Nijssen, R.C., ‘‘A novel reverse flow reactor coupling endothermic and exothermic reactions: an experimental study’’, Chemical Engineering Science, 2002, 4967–4985.
5. Arzamendi, G., Gania, L.M., Dieguez, P.M., Montes, M., Odriozola, J.A., Aguiar, E.F.S., ‘‘Computational fluid dynamics study of heat transfer in a microchannel reactor for low-temperature Fischer–Tropsch synthesis’’, Chemical Engineering Journal, 2010, 915–922.
6. Aubin, J., Prat, L., Xuereb, C., Gourdon, C., “Effect of microchannel aspect ratio on residence time distributions and the axial dispersion coefficient”, Chemical Engineering and Processing, 2009, 554-559.
7. Bakry, A., Salaymeh, A., Muhtaseb, A., Jrai, A., Trimis, D., ‘‘Adiabatic premixed combustion in a gaseous fuel porous inert media under high pressure and temperature: Novel flame stabilization technique’’, Fuel, 2011, 647–658.
8. Bhangale, A.S., Kundu, S., Wallace, W.E., Flynn, K.M., Guttman, C.M., Gross, R.A., Beers, K.L., ‘‘Continuous flow enzyme-catalysed polymerization in a microreactor’’, Journal of the American Society, 2011, 6006-6011.
9. Chan, S.H., Hoang, D.L., Ding, O.L., ‘‘Kinetic Modeling of Partial Oxidation of Methane in an Oxygen Permeable Membrane Reactor’’, Chemical Engineering Research and Design, 2005, 177–186.
10. Chan, F.L., Keith, J.M., ‘‘Designing reverse-flow packed bed reactors for stable treatment of volatile organic compounds’’, Journal of Environmental Management, 2006, 223–231.

11. Chen, G., Yuan, Q., Li, H., Li, S., ‘‘CO selective oxidation in a microchannel reactor for PEM fuel cell’’, Chemical Engineering Journal, 2004, 101-106.
12. Choi, C., Shin, J.S., Yu, D.I., Kim, M.H., ‘‘Flow boiling behaviors in hydrophilic and hydrophobic microchannels’’, 2011, 816–824.
13. Chu, J.C., Teng, J.T., Greif, R., ‘‘Experimental and numerical study on the flow characteristics in curved rectangular microchannels’’, 2010, 1558-1566.
14. Cittadini, M., Vanni, M., Barresi, A.A., Baldi, G., ‘‘Reverse-flow catalytic burners: response to periodical variationsin the feed’’, Chemical Engineering Science, 2001, 1443-1449.
15. Deshmukh, S.R., Vlachos, D.G., ‘‘A reduced mechanism for methane and one-step rate expressions for fuel-lean catalytic combustion of small alkanes on noble metals’’, Combustion and Flame, 2007, 366–383.
16. Feng, L., Liu, Z., Li, Y., ‘‘Numerical study of methane and air combustion inside a small tube with an axial temperature gradient at the wall’’, Applied Thermal Engineering, 2010, 2804-2807.
17. Gandia, L.M., Arzamendi, G., Montes, M., Centeno, M.A., Odriozola, J.A., Dieguez, P.M., ‘‘Integration of methanol steam reforming and combustion in a microchannel reactor for H_2 production: A CFD simulation study’’, 2009, 25–31.
18. Glockler, B., Kolios, G., Eigenberger, G., ‘‘Analysisofanovel reverse-flowreactorconceptforautothermal methane steamreforming’’, Chemical Engineering Science, 2003, 593–601.
19. Gokhale, S.V., Tayal, R.K., Jayaraman, V.K., Kulkarni, B.D., ‘‘Microchannel Reactors: Applications and Use in Process Development’’, International Journal of Chemical Reactor Engineering, 2005, 1-51.
20. Gosiewski, K., Bartmann, U., Moszczynski, M., Mleczko, L., ‘‘Effect of the intraparticle mass transport limitations on temperatureprofiles and catalytic performance of the reverse-flow reactor for thepartial oxidation of methane to synthesis gas’’,Chemical Engineering Science,1999, 4589-4602.
21. Gosiewski, K., Warmuzinski, K., ‘‘Effect of the mode of heat withdrawal on the asymmetry of temperature profiles in reverse-flowreactors. Catalytic combustion of methane as a test case’’, Chemical Engineering Science, 2007, 2679 – 2689.

22. Gosiewski, K., Matros, Y., Warmuzinski, K., Jaschik, M., Tanczyk, M., "Homogeneous vs. catalytic combustion of lean methane air mixtures in reverse-flow reactors", Chemical Engineering Science, 2008, 5010-5019.
23. Gosiewski, K., Pawlaczyk, A., Warmuzinski, K., Jaschik, M., "A study on thermal combustion of lean methane–air mixtures: Simplified reaction mechanism and kinetic equations", Chemical Engineering Journal, 2009, 9–16.
24. Guan, G., Kusakabe, K., Taneda, M., Uehara, M., Maeda, H., ''Catalytic combustion of methane over Pd-based catalyst supported on a macroporous alumina layer in a microchannel reactor'', Chemical Engineering Journal, 2008, 270–276.
25. Irani, M., Alizadehdakhel, A., Pour, A.N., Hoseini, N., ''CFD modeling of hydrogen production using steam reforming of methane in monolith reactors: Surface or volume-base reaction model?'', International journal of hydrogen energy, 2011, 1-9.
26. Karakaya, M., Avci, A.K., "Microchannel reactor modeling for combustion driven reforming of iso-octane", International journal of hydrogen energy, 2011, 6569- 6577.
27. Liauw, M.A., Walter, S., Malmberg, S., Schmidt, B., ''Comparison of microchannel and fixed bed reactors for selective oxidation reactions'', Chemical Engineering Research and Design, 2005, 1019-1029.
28. Liu, H., Dong, S., Li, B.W., Chen, H.G., ''Parametric investigations of premixed methane–air combustion in two-section porous media by numerical simulation'', Fuel, 2010, 1736–1742.
29. Liu, B., Hayes, R.E., Yi, Y., Mmbaga, J., Checkel, M.D., Zheng, M., ''Three dimensional modelling of methane ignition in areverse flow catalytic converter'',Computers and Chemical Engineering, 2007, 292–306.
30. Liu, Y., Cui, J., Jiang, Y.X., Li, W.Z., ''A numerical study on heat transfer performance of microchannels with different surface microstructures'', 2011, 921-931.
31. Marin, P., Hevia, M.A.G.,Ordonez, S., Diez, F.V., ''Combustion of methane lean mixtures in reverse flow reactors:Comparison between packed and structured catalyst beds'', Catalysis Today, 2005, 701–708.
32. Marin, P., Ordonez, S., Diez, F.V., ''Combustion of toluene–hexane binary mixtures in a reverse flow catalytic reactor'', Chemical Engineering Science, 2008, 5003 – 5009.

33. Marin, P., Ordonez, S., Diez, F.V., ‘‘Performance of reverse flow monolithic reactor for water–gas shift reaction’’, Catalysis Today, 2009, 185–190.
34. Men, Y., Kolb, G., Zapf, R., Pennemann, H., Hessel, V., ‘‘Total combustion of propane in a catalytic microchannel combustor’’, 2009, 91–96.
35. Ramdani, K., Pontier, R., Schweich, D., ‘‘Reverse flow reactor at short switching periods for VOC combustion’’, Chemical Engineering Science, 2001, 1531-1539.
36. Rouge, A., Spoetzl, B., Gebauer, B., Schenk, R., Renken, A., “Microchannel reactors for fast periodic operation: the catalytic dehydration of isopropanol”, Chemical Engineering Journal, 2001, 1419-1427.
37. Ruixiang, L., Yongqi, L., Zhenqiang, G., Bin, Z., ‘‘Simulation of Starting Up of a Reverse Flow Reactor for Thermal Oxidation of Lean Methane’’, Institute of Electrical and Electronics Engineers, 2009.
38. Salomons, S., Hayes, R.E., Poirier, M., Sapoundjiev, H., ‘‘Modelling a reverse flow reactor for the catalytic combustionof fugitive methane emissions’’, Computers and Chemical Engineering, 2004, 1599–1610.
39. Sotowa, K.I., Yamamoto, A., Nakagawa, K., Sugiyama, S., ‘‘Indentations and baffles for improving mixing rate in deep microchannel reactors’’, Chemical Engineering Journal, 2011, 490–495.
40. Triplett, K.A., Ghiaasiaan, S.M., Khalik, S.I., Sadowski, D.L., ‘‘Gas-liquid two-phase flow in microchannels Part I: two-phase flow patterns’’, 1999, 377-394.
41. Tullilah, M.B., Alajem, E., Gal, R., Sheintuch, M., ‘‘Flow-rate effects in flow-reversal reactors: experiments, simulationsand approximations’’,Chemical Engineering Science, 2003, 1135–1146.
42. Vlachos, D.G., Norton, D.G., ‘‘A CFD study of propane/air microflame stability’’, 2004, 97-107.
43. Wan, Y.S.S., Gavriilidis, A., Yeung, K.L., ‘‘1-pentene epoxidation in titanium silicalite-1 microchannel reactor: experiments and modelling’’, 2003.
44. Wierzchowski, P.T., Zatorski, L.W., ‘‘Kinetics of catalytic oxidation of carbon monoxide and methane combustion over alumina supported Ga_2O_3, SnO_2 or V_2O_5’’, Applied Catalysis, 2002, 53-65.

45. Zhang, L., Ju, J., Zeng, C., Xu, N., ‘‘Continuous synthesis of zeolite NaA in a microchannel reactor’’, Chemical Engineering Journal, 2006, 115–121.
46. Zhang, J., Vitzthum, V.B., Marquaire, P.M., Wild, G., Commenge, J.M., “Direct conversion of methane in formaldehyde at very short residence time”, Chemical Engineering Science, 2011, 6331-6340.
47. Zhenqiang, G., Chengguan, W., Yongqi, L., Ruixiang, L., ‘‘Simulation of Convection Heat Transfer in Thermal Flow Reversal Reactor for Lean Methane Oxidation’’, 2009, 403-406.